NASA TECHNICAL NOTE

NASA TN D-3088

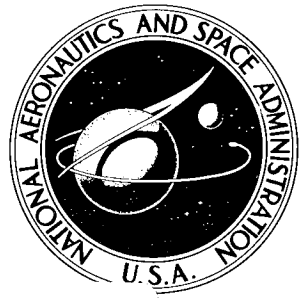

AERODYNAMIC CHARACTERISTICS OF SPHERICALLY BLUNTED CONES AT MACH NUMBERS FROM 0.5 TO 5.0

by Robert V. Owens

George C. Marshall Space Flight Center
Huntsville, Ala.

NATIONAL AERONAUTICS AND SPACE ADMINISTRATION - WASHINGTON, D. C. - DECEMBER 1965

NASA TN D-3088

AERODYNAMIC CHARACTERISTICS OF SPHERICALLY BLUNTED CONES AT MACH NUMBERS FROM 0.5 TO 5.0

By Robert V. Owens

George C. Marshall Space Flight Center
Huntsville, Ala.

NATIONAL AERONAUTICS AND SPACE ADMINISTRATION

For sale by the Clearinghouse for Federal Scientific and Technical Information
Springfield, Virginia 22151 – Price $3.00

TABLE OF CONTENTS

LIST OF ILLUSTRATIONS

LIST OF ILLUSTRATIONS (Cont'd)

LIST OF ILLUSTRATIONS (Cont'd)

LIST OF ILLUSTRATIONS (Cont'd)

DEFINITION OF SYMBOLS

Symbol	Definition
A	Area based on diameter D, (in^2)
C_{D_b}	Base drag coefficient $\left(\frac{P-P_b}{q}\right)$
C_{D_f}	Fore drag coefficient ($C_{D_t} - C_{D_b}$)
C_{D_t}	Total drag coefficient $\left(\frac{D_t}{qA}\right)$
C_N	Normal force coefficient slope $\left(\frac{1}{rad}\right)$
D_t	Total drag (lb)
D	Base diameter (in.)
d	Diameter of spherical nose segment at station of tangency (d/2r)
$\frac{d}{D}$	Bluntness ratio
ϵ	Cone half angle (deg.)
L	Length of body
L/D	Fineness ratio
M	Mach number
M_s	Minimum Mach number for shock attachment for pointed cones
N	Normal force (lb.)
P	Free stream static pressure (psi)
P_b	Base pressure (psi)
P_t	Total pressure (psi)
q	Dynamic pressure (psi)

DEFINITION OF SYMBOLS (Cont'd)

Symbol	Definition
R_n	Reynolds number $\left(\frac{\rho VL}{\mu}\right)$
r	Radius of spherical nose (in.)
T_t	Total temperature (° F)
CP/D	Center of pressure location (from base)
α	Angle of attack (deg.)

AERODYNAMIC CHARACTERISTICS OF SPHERICALLY BLUNTED CONES AT MACH NUMBERS FROM 0.5 TO 5.0

SUMMARY

12138

An experimental investigation has been made to determine the aerodynamic characteristics of several cones at Mach numbers from 0.5 to 5.0 and to establish the effects of bluntness. The results of the investigation show that the abrupt changes in aerodynamic parameters in the transonic region are closely related to the development of the shock wave pattern. Those parameters most affected were the normal force coefficient slope and the forebody drag coefficient. The center of pressure, on the other hand, remained relatively stationary for cones with moderate half-angles, except at very near sonic Mach number. The effects of bluntness were minimal at Mach numbers smaller than those required for shock attachment on pointed cones. At higher Mach numbers, bluntness effects were sizeable for the smaller cone half-angles, but negligible for the larger ones. In every case, increases in bluntness as well as cone angle increased the downstream movement of the center of pressure.

INTRODUCTION

The inadequacy of theory in predicting the aerodynamic characteristics of blunted cones accurately creates a need for a thorough experimental investigation. Such a study has been especially desirable in the transonic Mach number range where no practical theory applies.

This experimental program was initiated to satisfy this need and to provide designers of blunted-cone vehicles with data from a wide range of parametric variations. The normal force coefficient slopes, center of pressure locations, and forebody drag coefficients were determined for twelve cones over a Mach number range from 0.5 to 5.0. The models used in the investigation were grouped into four families of different cone angles, each having three different nose bluntness ratios. Eight models with two additional bluntness ratios were tested up to M= 2.0 [1]. From this wide range of geometric parameters, the effects of bluntness and cone angle could be deduced in addition to those of Mach number. The tests were conducted at the NASA, Marshall Space Flight Center, 14 x 14-inch trisonic and the 7 x 7-inch supersonic wind tunnels.

MODELS AND APPARATUS

The investigation was conducted in three series of tests. Transonic and supersonic tests were run in the trisonic wind tunnel over Mach number ranges from 0.47 to 1.93 and 2.74 to 4.96, respectively. To establish the continuity and validity of the data, a supersonic test covering the Mach range from 1.58 to 4.39 was conducted in the 7 x 7-inch supersonic wind tunnel. The characteristic air properties during operation of both facilities are given in Table 1.

TABLE I

TEST CONDITIONS

Wind Tunnel Test Facility	M	P_t (psia)	T_t (°F)	R_n/in. x 10^{-6}
14 x 14 Transonic	0.5	22	120	0.352
	0.7	↓	↓	0.436
	0.85			0.489
	0.95			0.510
	1.15			0.535
	1.25	↓		0.535
	1.43	22	↓	0.513
	1.93	28	120	0.590
14 x 14 Supersonic	2.74	30	120	0.402
	2.99	45	120	0.551
	3.48	75	140	0.657
	4.00	105	140	0.717
	4.45	105	180	0.551
	4.96	105	200	0.402
7 x 7 Supersonic	1.58	14.5	90	0.350
	1.99	↓	↓	0.306
	2.44			0.246
	2.99			0.187
	3.26			0.162
	3.60			0.137
	3.89	↓	↓	0.117
	4.39	14.5	90	0.094

Twelve cone models representing four families of different cone half-angles of 10, 13.32, 25, and 50 degrees were tested at all of the above Mach number ranges. The three cones within each family had bluntness ratios of 0, 0.4, and 0.8; i.e., one was pointed, while the other two were truncated and tipped with spherical segments. Eight models, representing two additional bluntness ratios (d/D = 0.2 and 0.6) for each of the cone families, were tested in only the Mach number range from 0.43 to 1.93.[1] The geometric characteristics of the models and nomenclature are given in Figure 1, and the configurations tested are represented in the diagrams of Figure 2. Some representative Schlieren pictures of the test models are shown in Figure 3 for various Mach numbers.

All models were mounted on a sting which contained a system of interchangeable strain gauge beams as parts of a three-component balance. Because of limitations on the model size, the balance system used in the 7 x 7-inch tunnel test was housed within a faired portion of the sting aft of the model base. The balance assembly of the 14 x 14-inch tunnel, however, could be fitted conventionally to the forward end of the sting projecting into the models. Composition X-ray pictures of both balance systems are shown in Figures 4 and 5.

ACCURACY OF DATA

All force and base pressure measurements were taken over the angle of attack range from approximately -4° to 10°, which was traversed automatically in both tunnel facilities. Because of the sting effects on base pressures, the accuracy of the total drag is somewhat uncertain. By subtracting the base drag, which was determined from a base pressure measurement, the invalid component is removed. The resulting fore drag, which consists of wave drag and skin friction drag, should be accurate at the designated Reynolds numbers.

Data reduction of the strain gauge and base pressure readings were achieved through digitizing the analog signals, punching values into data cards, and finally processing the card data into coefficient form by computer.

The accuracy of the data, estimated by several means, takes into consideration the following:

a. Data scatter
b. Repeatability of a given test point
c. Agreement of data measured by several different strain gauges
d. Level of accuracy of previous tests
e. Continuity between the data from the two different test facilities.

Based on these indications, the estimated accuracy of the faired data is

$$\frac{CP}{D} = \pm 0.02, \qquad CN = \pm 0.04, \qquad C_{D_f} = \pm 0.01.$$

RESULTS AND DISCUSSION

The results of the test are presented in a manner to enable the study of the variation of normal force coefficient slope, center of pressure, and forebody drag coefficient with Mach number for various cone configurations and also to show the effects of cone half-angle (ϵ) and bluntness (d/D). The basic data variations with Mach number are given in Figures 7 through 15 for various cone half-angles and are grouped according to bluntness. To provide data for the lower end of the Mach number spectrum, the results of the transonic test published earlier[1] are included. Results from various other sources[2,3] are also incorporated when possible. The interpolated values for various intermediate cone half-angles, represented by dashed lines, are also indicated in the above figures. By presenting cross-plots of the aerodynamic characteristics versus cone half-angles at various Mach numbers (Figures 16 through 37), the effects of cone angle and bluntness can be studied directly. Here again the data from other sources, notably from Reference 3, provided complementing key points.

Normal Force Coefficient Slope

With a few exceptions, the linearity of normal force coefficient with angle of attack was maintained to approximately ±4 degrees. The normal force coefficient slopes at zero angle of attack are presented in Figures 7 through 9 for three degrees of bluntness. For zero bluntness cones, the values of normal force coefficient slope remain relatively constant once the local flow becomes supersonic, and the levels agree well with hypersonic Newtonian theory, even for Mach numbers less than 5.0. For blunted cones, however, the values of normal force coefficients slope for moderate cone half-angles decline at the beginning of the supersonic Mach number range, but tend to remain constant or increase slightly at the end of the test Mach number range. An increase in C_N values with still higher Mach numbers would be necessary to obtain agreement with hypersonic Newtonian values.

For Mach numbers smaller than M_s (minimum Mach number for shock attachment for pointed cone), no significant changes in $C_{N\alpha}$ were observed as the bluntness was increased from 0 to 0.4. For cones up to $\epsilon = 30°$, bluntness ratios

of 0.8, however, produced very pronounced $C_{N\alpha}$ peaks which occurred approximately at those Mach numbers identified with shock attachment on pointed cones.

The cross-plots of $C_{N\alpha}$ versus cone half-angles at various Mach numbers are shown in Figures 16 through 23. In general, bluntness effects were very small for subsonic Mach numbers, but became sizeable at $M > M_s$ for all cone half-angles, except $\epsilon = 50°$.

Center of Pressure

Since both the normal force coefficient and pitching moment coefficient were generally linear up to ±4° angle of attack, the variation of the center of pressure with angle of attack was nearly negligible in that range. The values of the cone centers of pressure at zero angles of attack are presented in Figures 10 through 12 for bluntness ratios 0, 0.4, and 0.8. The least change of center of pressure with Mach number was exhibited by the $\epsilon = 25°$ cone family. For all others, a downstream or upstream movement of the center of pressure was observed in the sonic Mach number region with a subsequent stabilization beginning at the transition of local flow from transonic to supersonic speeds.

Figures 24 through 30 show center of pressure locations versus cone half-angles at various Mach numbers. Up through free stream transonic Mach numbers, the effect of bluntness was greatest for small cone half-angles and decreased gradually with increasing cone angle. While a bluntness increase from 0 to 0.8 at Mach 0.68 caused the center of pressure of the $\epsilon = 10°$ cone family to move approximately 0.55 diameters downstream, the same bluntness increase on the $\epsilon = 25°$ cones resulted in a downstream CP/D movement of only 0.25 diameters.

For higher Mach numbers, the bluntness effect is largest for $\epsilon \approx 10°$; then it reaches a minimum for cone half angles of about 40°, and tends to increase again for $\epsilon = 50°$. The agreement at $M = 4.0$ of the center of pressure values with the relationship,

$$\frac{X_{CP}}{D} = \frac{L}{D} \left[1 - 2/3 \sec^2 \epsilon\right] ; \alpha = 0,$$

is good for all pointed cones, except those of $\epsilon = 50°$. This equation assumes constant pressure along a surface element, which is the case for cones in supersonic flow. Reference 4 substantiates that the local flow regime for cones of $\epsilon = 50°$ is still transonic up to a freestream Mach number of 4.0.

For cones with $\epsilon > 35°$, the centers of pressure are located downstream of the base under all conditions. Because the center of pressure is defined as the ratio of pitching moment to the normal force, unsymmetrical axial force distribution at

angles of attack generates a stabilizing couple of sufficient magnitude to shift the center of pressure off the body.

Forebody Drag Coefficents

The zero angle of attack drag coefficients presented in this report contain only forebody wave drag and skin friction coefficients.

Figures 13 through 15 show the variation of the forebody drag coefficient with Mach number for three degrees of bluntness. The initial drag rise is nearly identical for all bluntness ratios up to the shock attachment Mach numbers for a given cone half-angle. For cones with bluntness ratios up to 0.4, the maximum drag coefficients for a given cone occur at M_s, while peak values for larger bluntness ratios occur at higher Mach numbers. For comparison, the hypersonic Newtonian drag values are included which were determined from

$$C_{D_o} = (1+\sin^2 \epsilon)\left(\frac{d}{D}\right)^2 + 2 \sin^2 \epsilon \left[1-\left(\frac{d}{D}\right)^2\right].$$

The first term in this equation represents the drag resulting from the spherical segment; the second term is the drag due to the truncated remainder of the cone.

In general, the effects of bluntness on the forebody drag coefficient of a given cone are negligible for $M < M_s$, but are large at $M > M_s$ and small cone half-angles (see Figures 31 through 37). For cone half-angles of $\epsilon = 40°$ and larger, the bluntness effects are almost negligible at all Mach numbers.

Abrupt variations of the data with Mach number occur for nearly all cones regardless of bluntness. These phenomena are closely related to the mechanism of the shock wave development in the transonic region. This process, illustrated in the diagrams of Figure 6 for pointed cones, is qualitatively described as follows:

> As the free stream Mach number increases from subsonic values, a sonic line forms at the shoulder of the cone, together with a main shock (nearly normal) at the beginning of the wake. This marks the beginning of the transonic range, which encompasses all free stream Mach numbers from the instant the highest local Mach number reaches unity.[5] As Mach number increases, the main shock grows and tends to move downstream, while at the same time a second shock wave approaches the cone vertex in the stream direction. Finally, this bow wave, whose shape and stand-off distance depend on the geometry of the cone and the Mach number attaches while retaining some of its curvature. The conditions behind the shock are subsonic; this means that the downstream flow field (especially

at the shoulder) influences the entire shock. However, with further increase in Mach number, a value is reached for which conditions behind the shock cease to be subsonic. The shock angle decreases while the shock becomes straight. Under the latter circumstances, the flow about the cone is genuinely supersonic, and therefore, the shock is independent of the downstream flow field. Further increases in Mach number thus affect the data very little.

The span of transonic Mach numbers for pointed cones varies according to the cone geometry; thus, for $\epsilon = 10°$ the transonic regime extends from about $M = 0.9$ to $M = 1.15$, while for $\epsilon = 50°$ it may range from $M = 0.7$ to $M = 4.0$ or higher. Consequently, considerable data changes are seen in these ranges.

The flow field development around blunted cones is considerably more complex. On small half-angle cones, the expansion around the rounded tip causes local supersonic flow at free stream $M < 1.0$. This supersonic flow is then altered by shocking back to subsonic flow. At high Mach numbers with the 50° cone at a bluntness of 0.8, subsonic flow undoubtedly exists all the way to the base because of the strong normal shock. Thus, shock and flow development around blunted cones is not nearly so straightforward.

CONCLUSIONS

From the results of the investigation to determine the aerodynamic characteristics of blunted cones, the following general conclusions are formed.

1. The effect of bluntness on the forebody drag coefficient is small for all cones at Mach numbers less than those required for shock attachment on pointed cones. This is generally true for the normal force coefficient slope, except at small cone half-angles and extreme bluntness.

2. For Mach numbers higher than M_s, the forebody drag coefficient and the normal force coefficient slope are greatly influenced by bluntness.

3. For cones with half-angles less than 30°, the center-of-pressure locations are more sensitive to bluntness than to Mach number changes. For cones with $\epsilon > 35°$, the centers of pressure are located downstream of the base under all conditions and are influenced by changes in Mach number as well as bluntness.

4. With the exception of normal force coefficient slopes for the blunted cones, the aerodynamic parameters for supersonic Mach numbers are, in most cases, closely approximated by Newtonian theory for hypersonic flow.

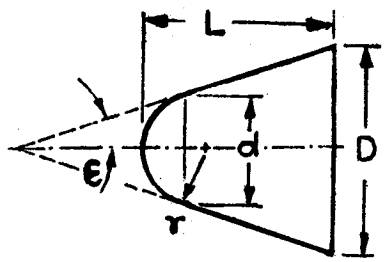

D Base diameter

r Nose radius

L Length of body

d Diameter at tangent station

ϵ Cone half angle

TUNNEL	DIAMETER OF MODELS
14 x 14-inch	3.00 in.
7 x 7-inch	1.50 in.

CONFIG.	ϵ	d/D	r/D	a/A	L/D
A-1	10°	0	0	0	2.836
A-2	10°	0.2	0.102	0.04	2.352
A-3	10°	0.4	0.203	0.16	1.869
A-4	10°	0.6	0.305	0.36	1.386
A-5	10°	0.8	0.406	0.64	0.903
B-1	13.32°	0	0	0	2.112
B-2	13.32°	0.2	0.103	0.04	1.768
B-3	13.32°	0.4	0.206	0.16	1.425
B-4	13.32°	0.6	0.308	0.36	1.082
B-5	13.32°	0.8	0.411	0.64	0.739
C-1	25°	0	0	0	1.077
C-2	25°	0.2	0.110	0.04	0.922
C-3	25°	0.4	0.221	0.16	0.771
C-4	25°	0.6	0.331	0.36	0.620
C-5	25°	0.8	0.441	0.64	0.469
D-1	50°	0	0	0	0.420
D-2	50°	0.2	0.156	0.04	0.372
D-3	50°	0.4	0.311	0.16	0.325
D-4	50°	0.6	0.467	0.36	0.277
D-5	50°	0.8	0.622	0.64	0.230

FIGURE 1. NOMENCLATURE AND MODEL CHARACTERISTICS

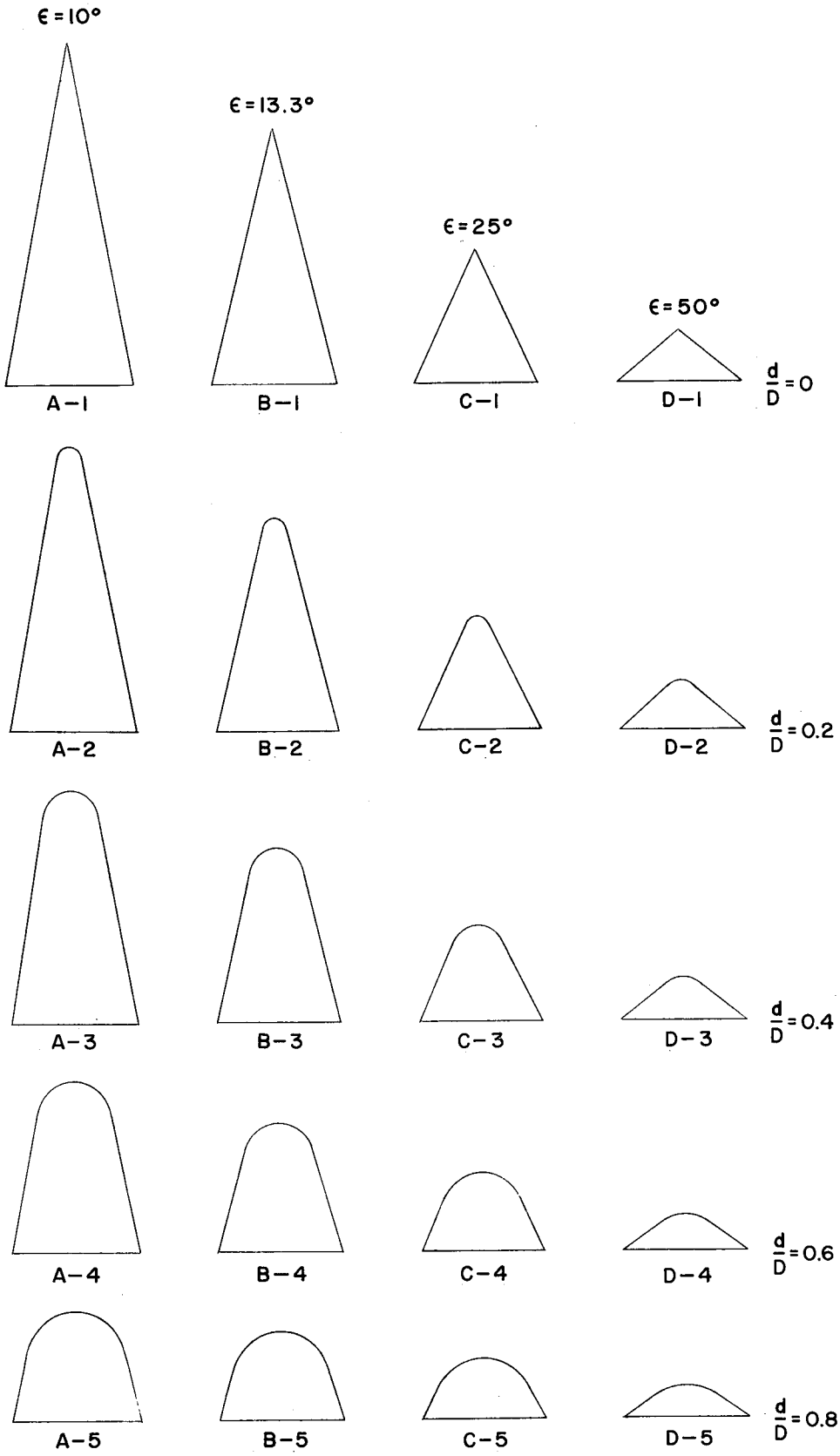

FIGURE 2. CONE FAMILIES TESTED

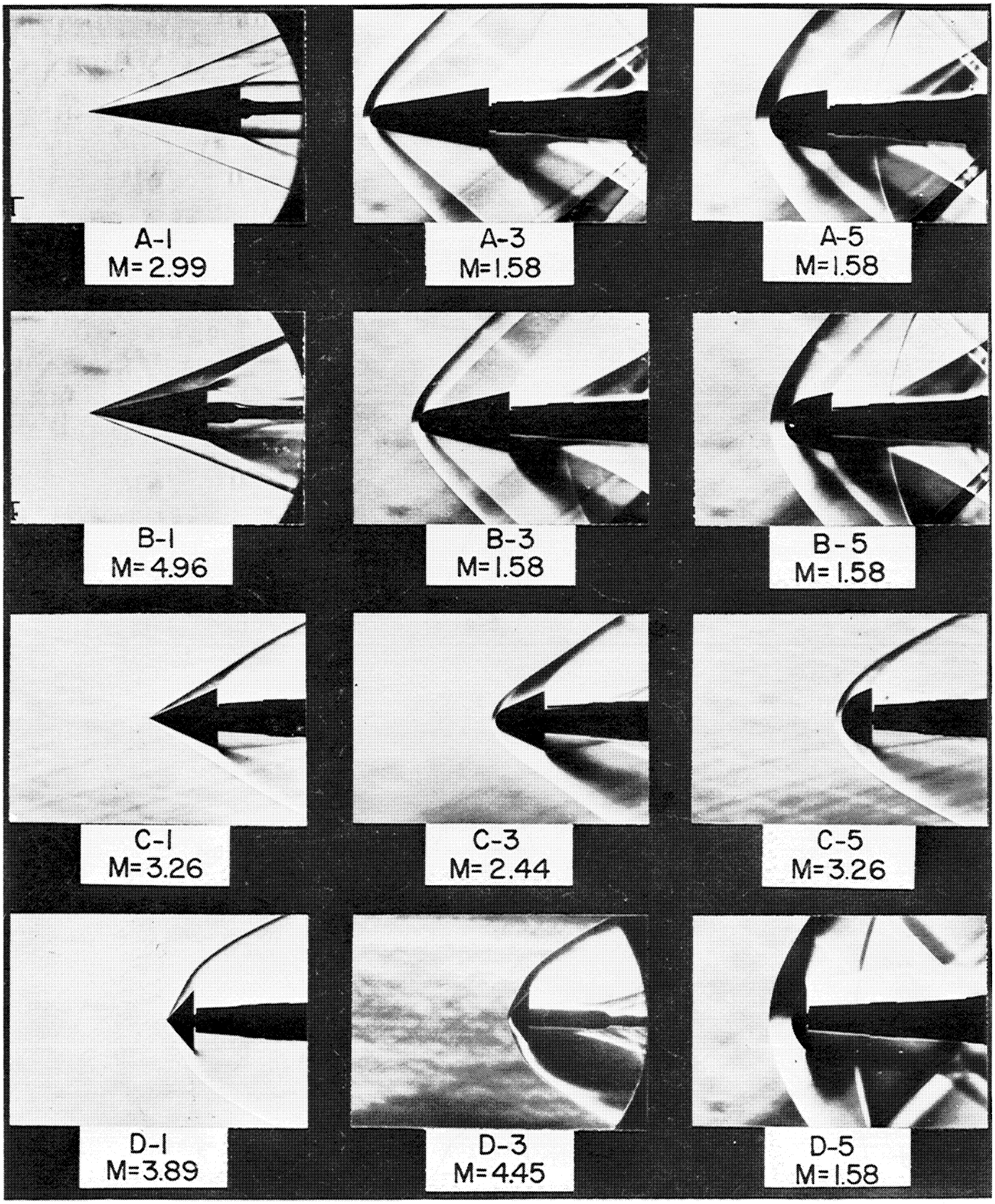

FIGURE 3. TYPICAL SCHLIERENS

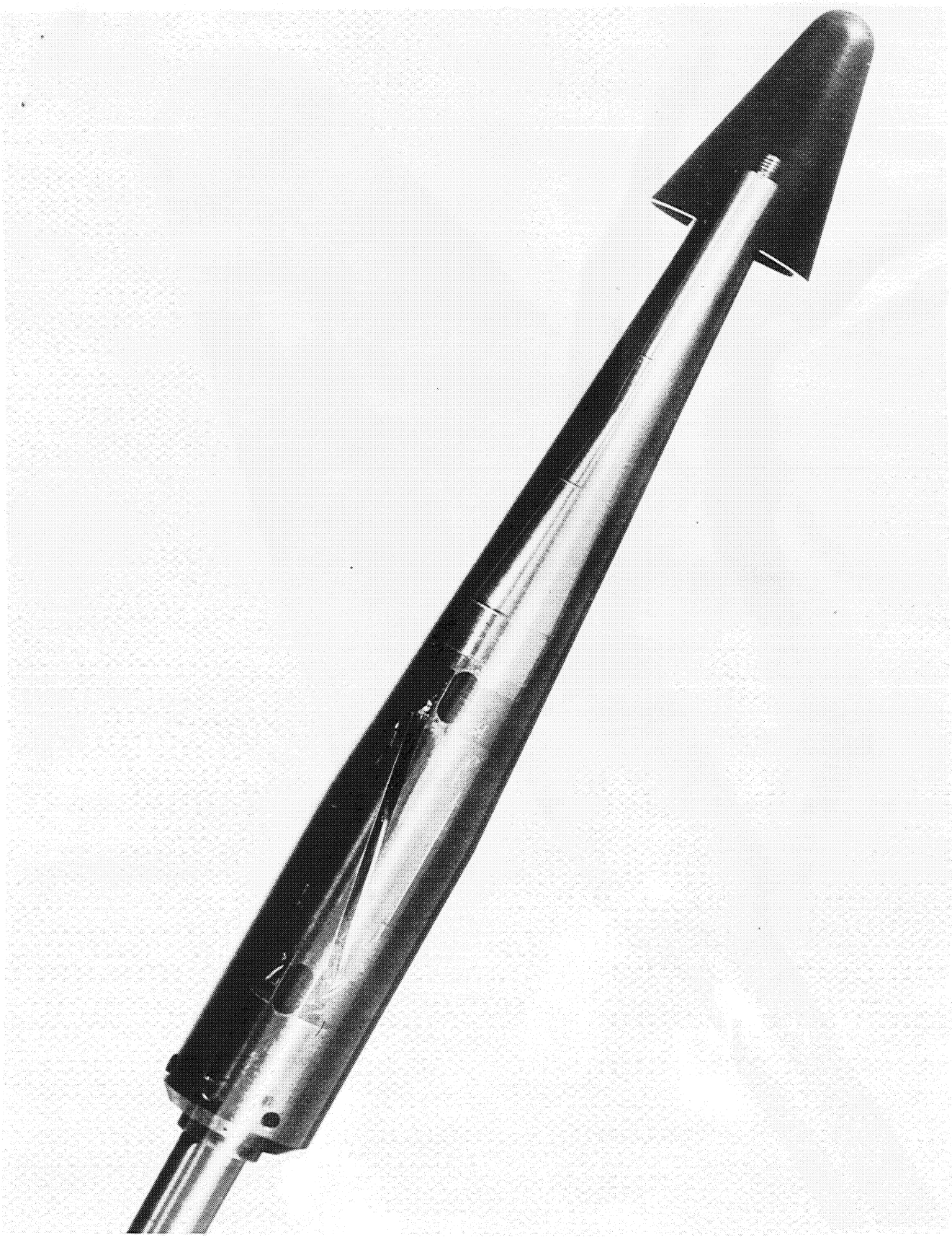

FIGURE 4. MODEL & BALANCE SYSTEM USED IN 7 X 7-INCH TUNNEL TESTS

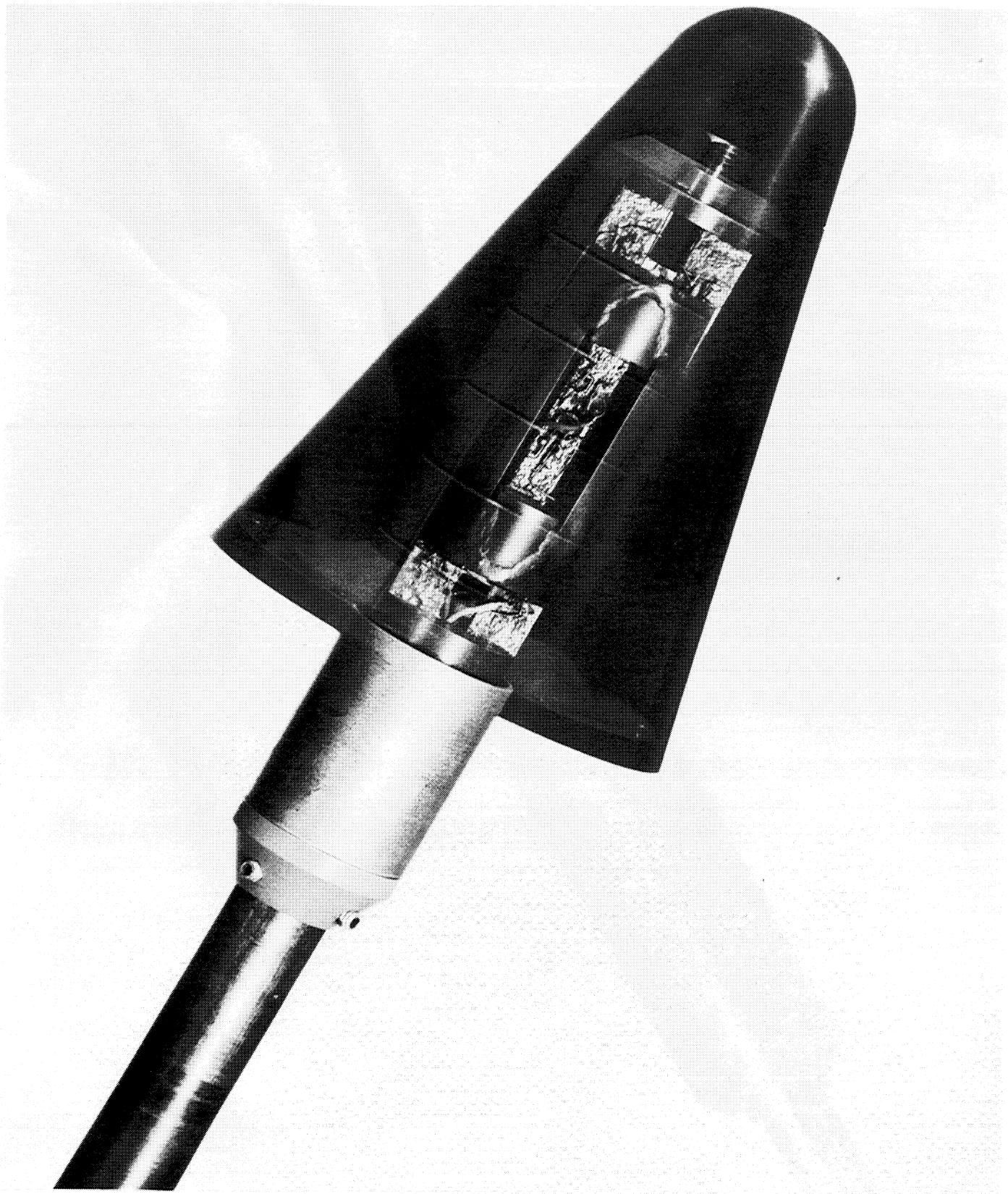

FIGURE 5. MODEL AND BALANCE SYSTEM USED IN 14 X 14-INCH TUNNEL TESTS

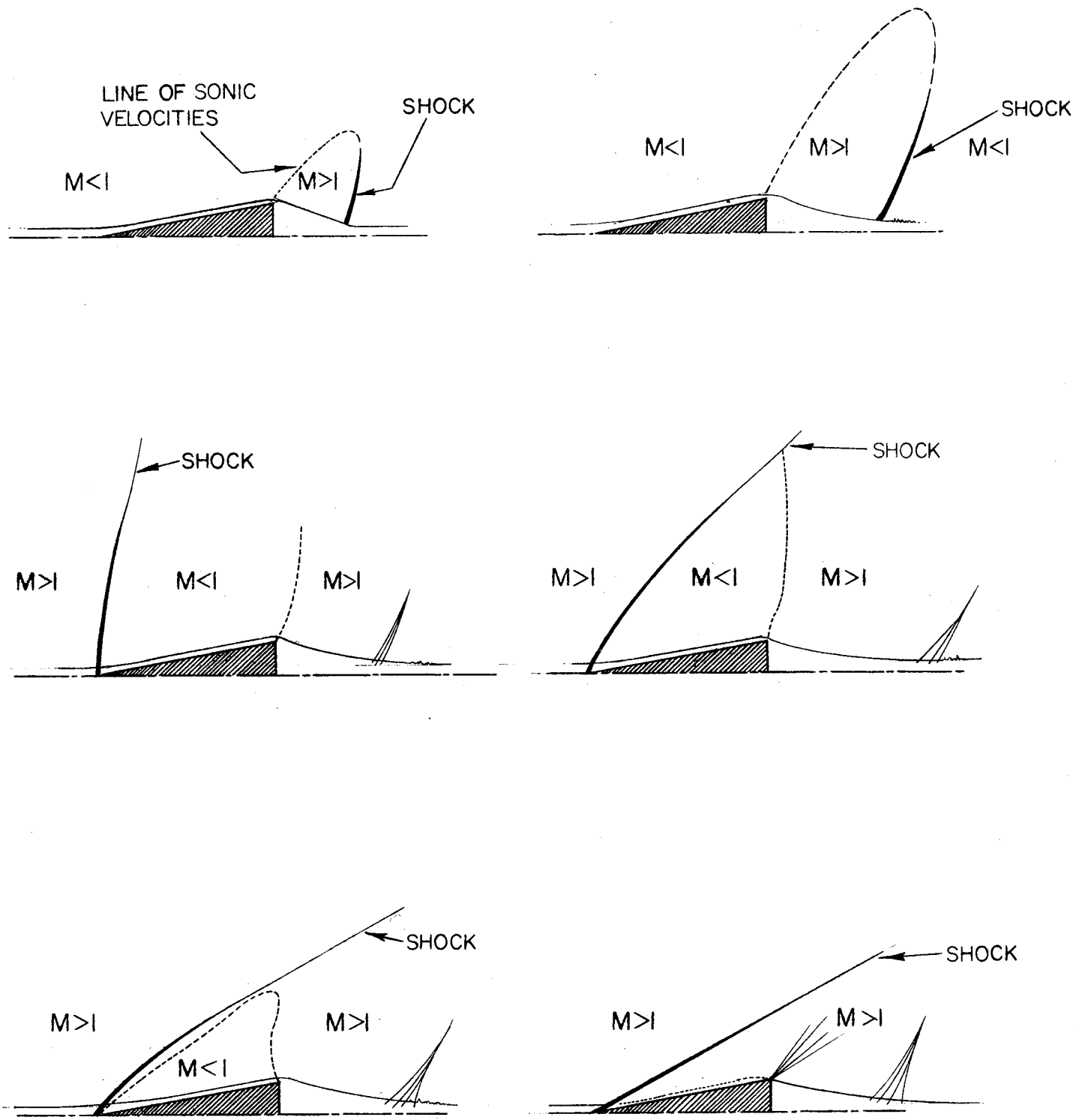

FIGURE 6. DIAGRAMMATIC REPRESENTATION OF TRANSONIC FLOW CONFIGURATIONS FOR CONES

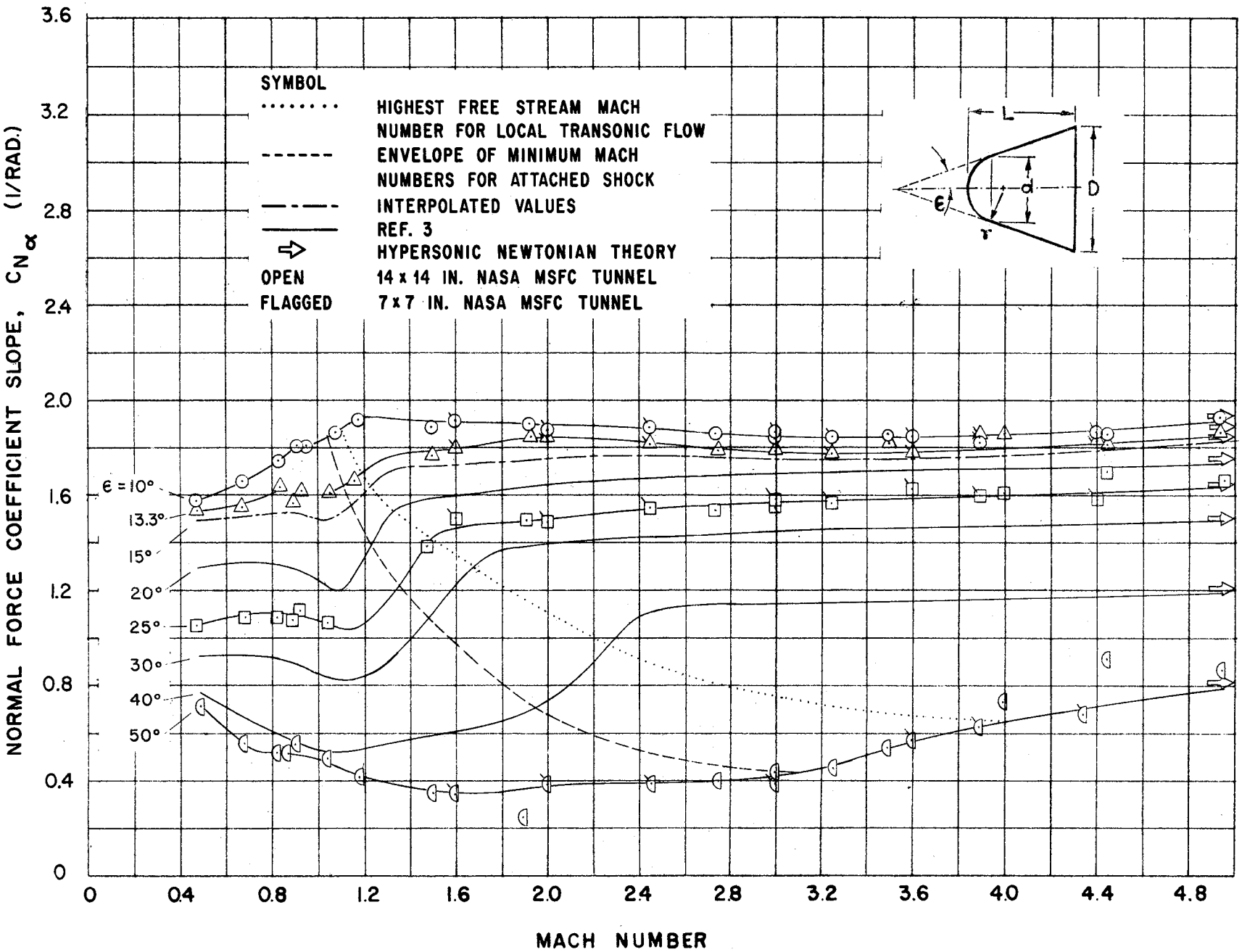

FIGURE 7. VARIATION OF NORMAL FORCE COEFFICIENT SLOPE WITH MACH NUMBER FOR VARIOUS CONES (d/D = 0)

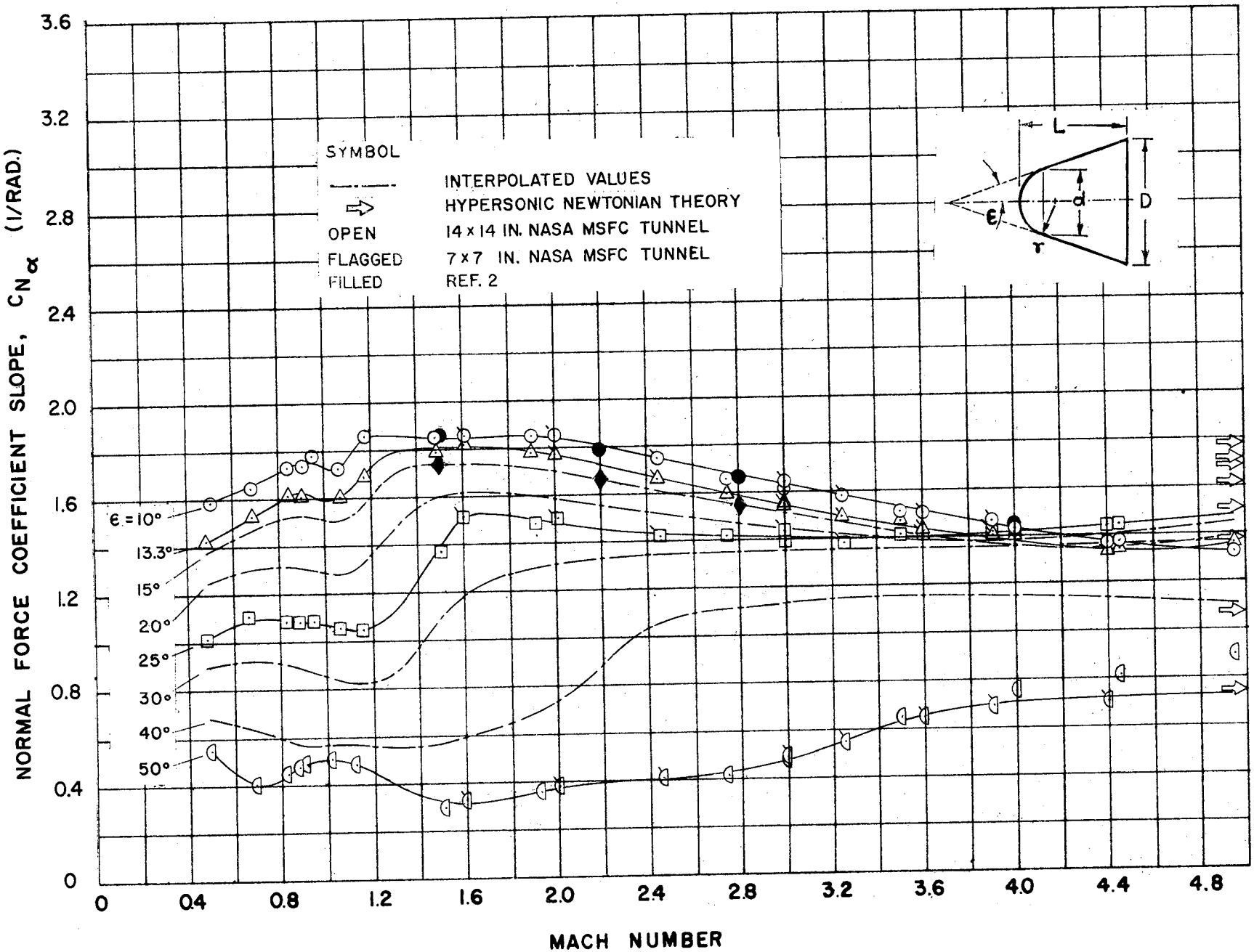

FIGURE 8. VARIATION OF NORMAL FORCE COEFFICIENT SLOPE WITH MACH NUMBER FOR VARIOUS CONES(d/D = 0.4)

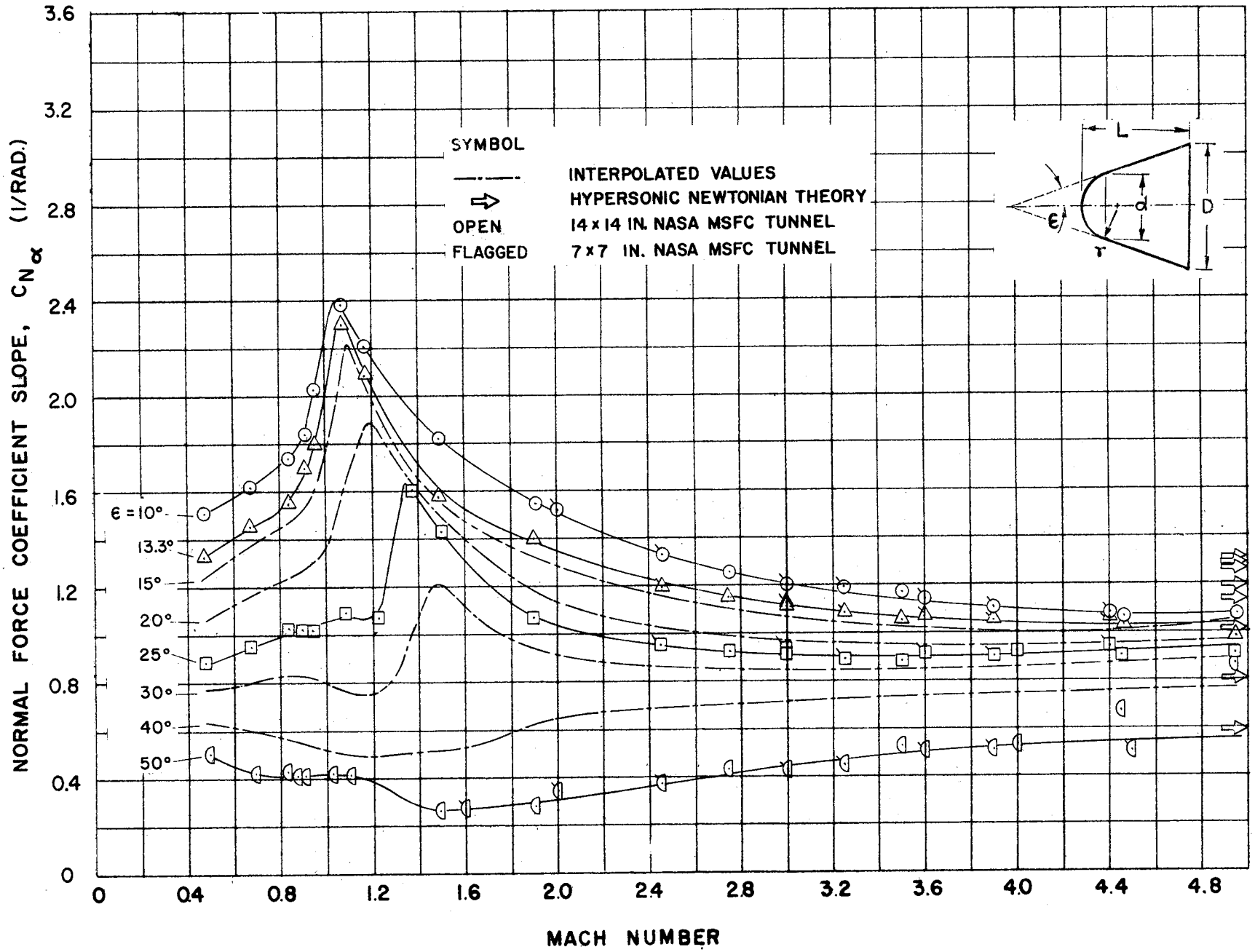

FIGURE 9. VARIATION OF NORMAL FORCE COEFFICIENT SLOPE WITH MACH NUMBER FOR VARIOUS CONES (d/D = 0.8)

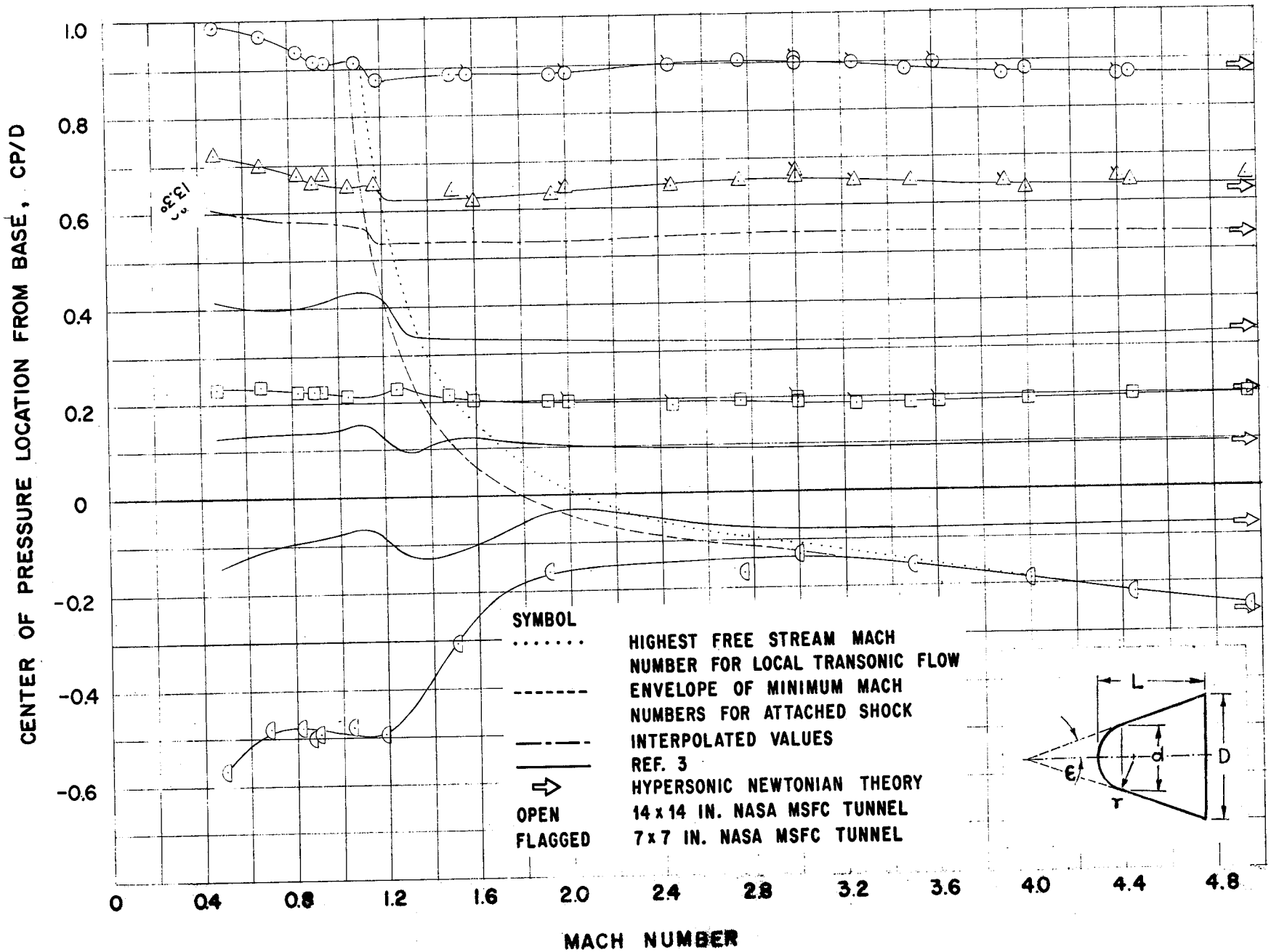

FIGURE 10. VARIATION OF CENTER OF PRESSURE WITH MACH NUMBER FOR VARIOUS CONES (d/D = 0)

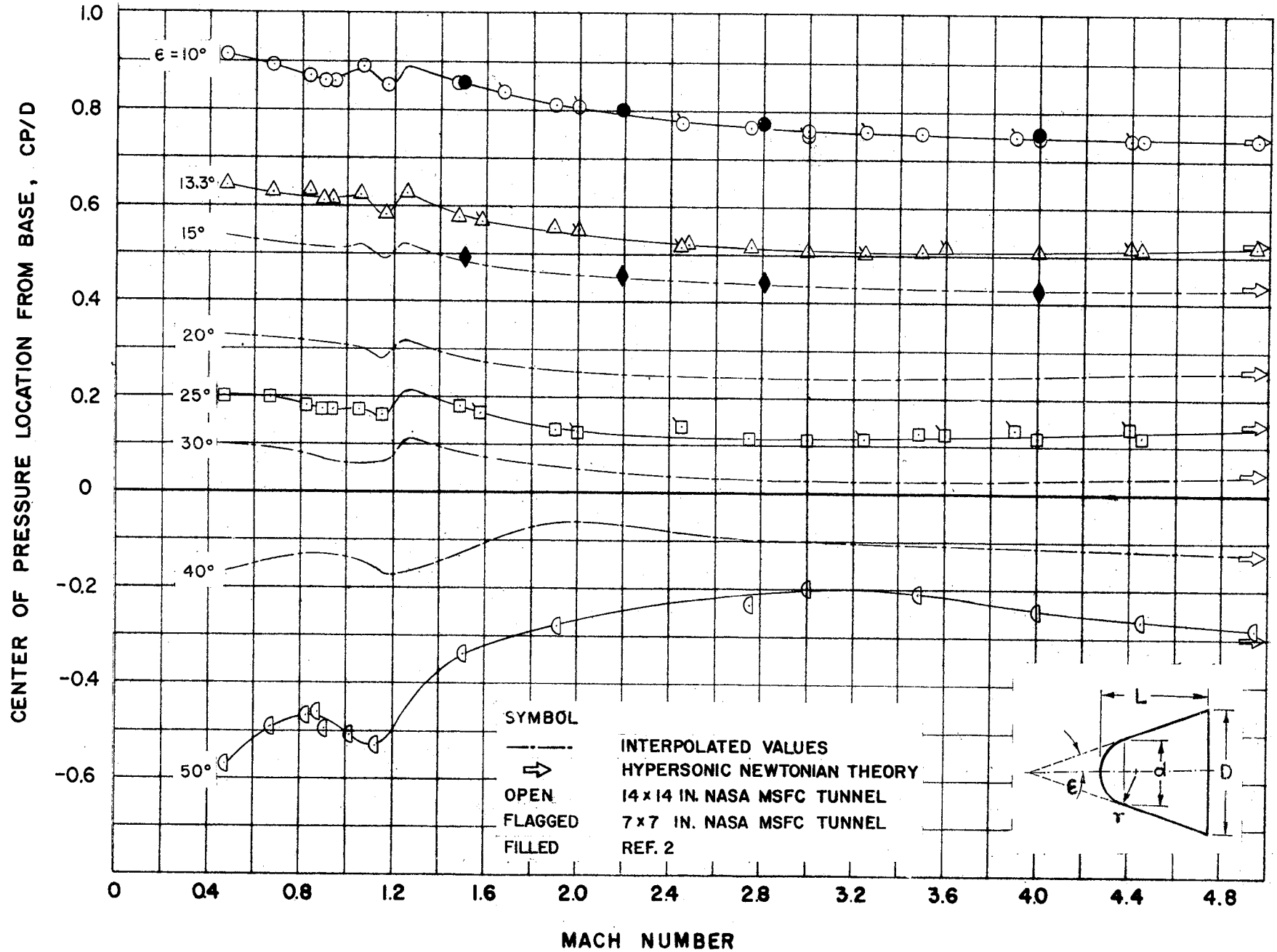

FIGURE 11. VARIATION OF CENTER OF PRESSURE WITH MACH NUMBER FOR VARIOUS CONES (d/D = 0.4)

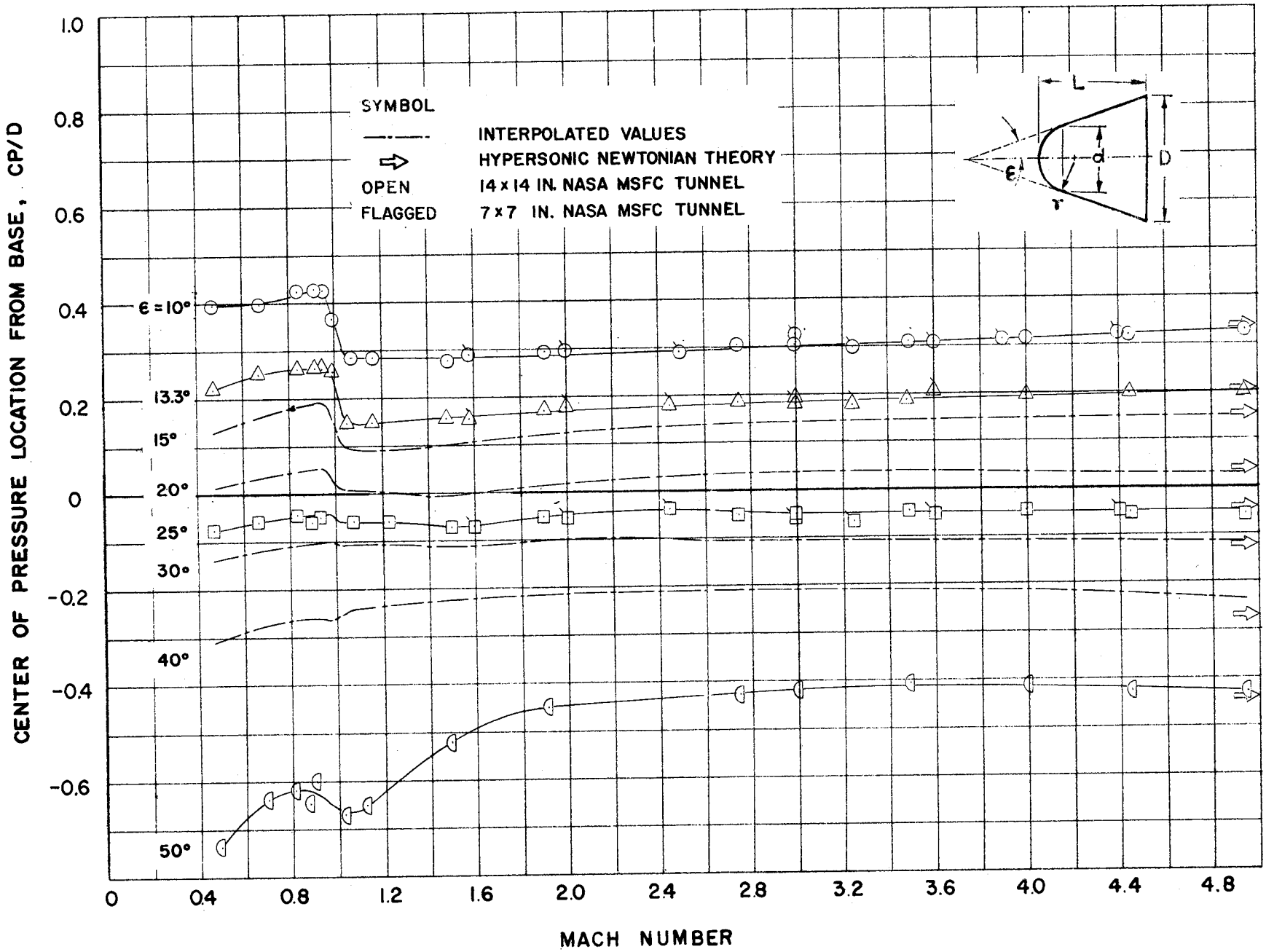

FIGURE 12. VARIATION OF CENTER OF PRESSURE WITH MACH NUMBER FOR VARIOUS CONES (d/D = 0.8)

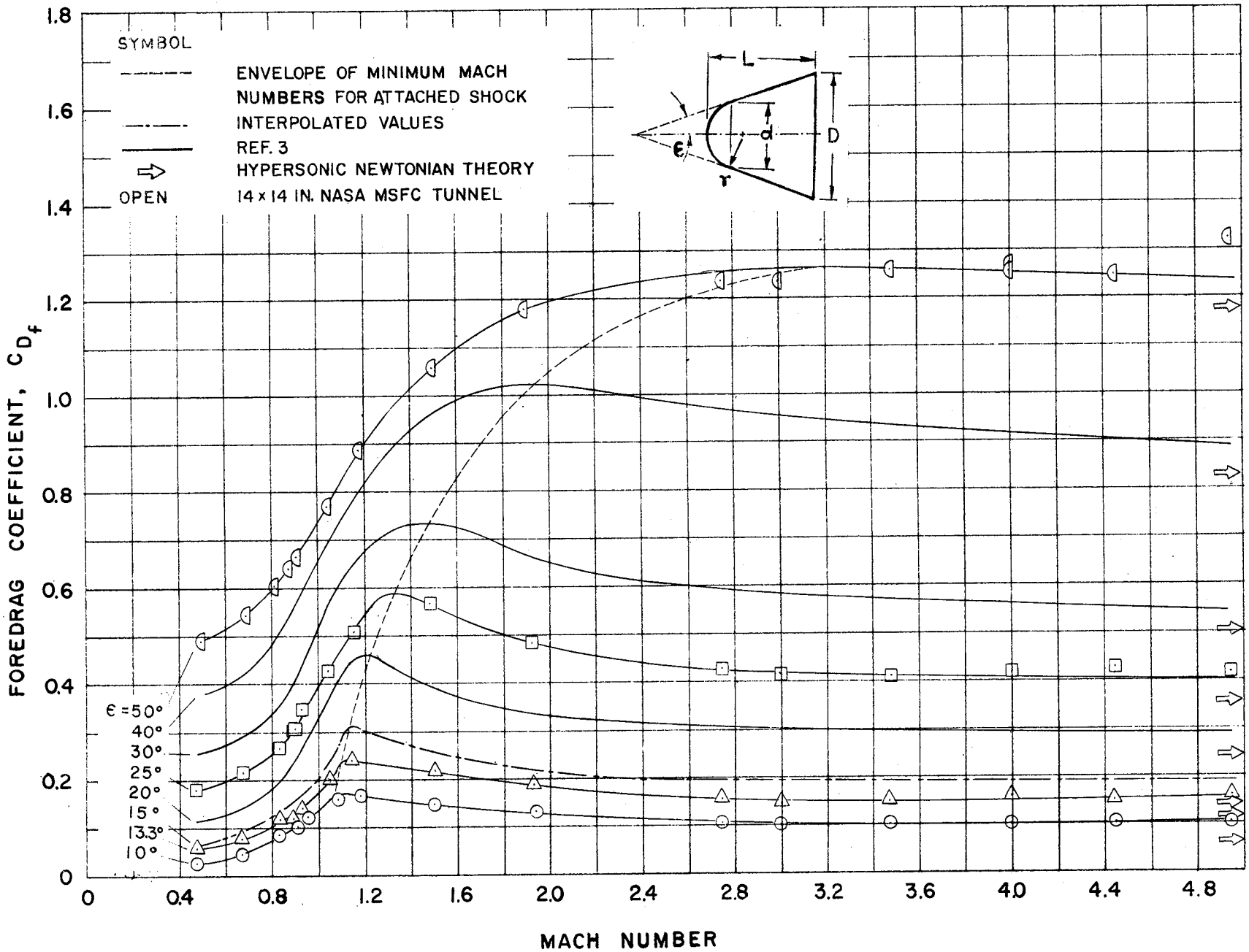

FIGURE 13. VARIATION OF FOREDRAG COEFFICIENT WITH MACH NUMBER FOR VARIOUS CONES (d/D = 0)

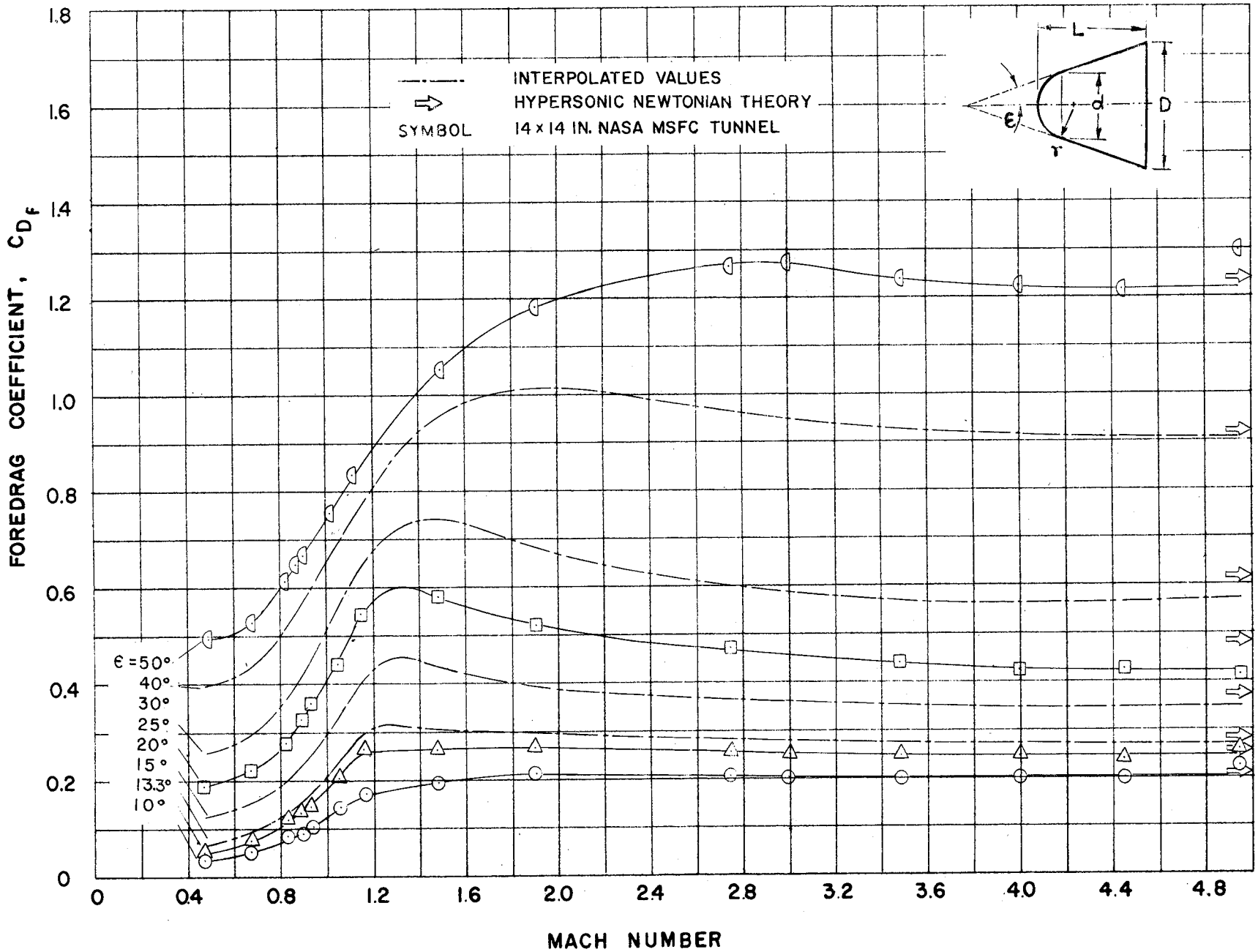

FIGURE 14. VARIATION OF FOREDRAG COEFFICIENT WITH MACH NUMBER FOR VARIOUS CONES (d/D = 0.4)

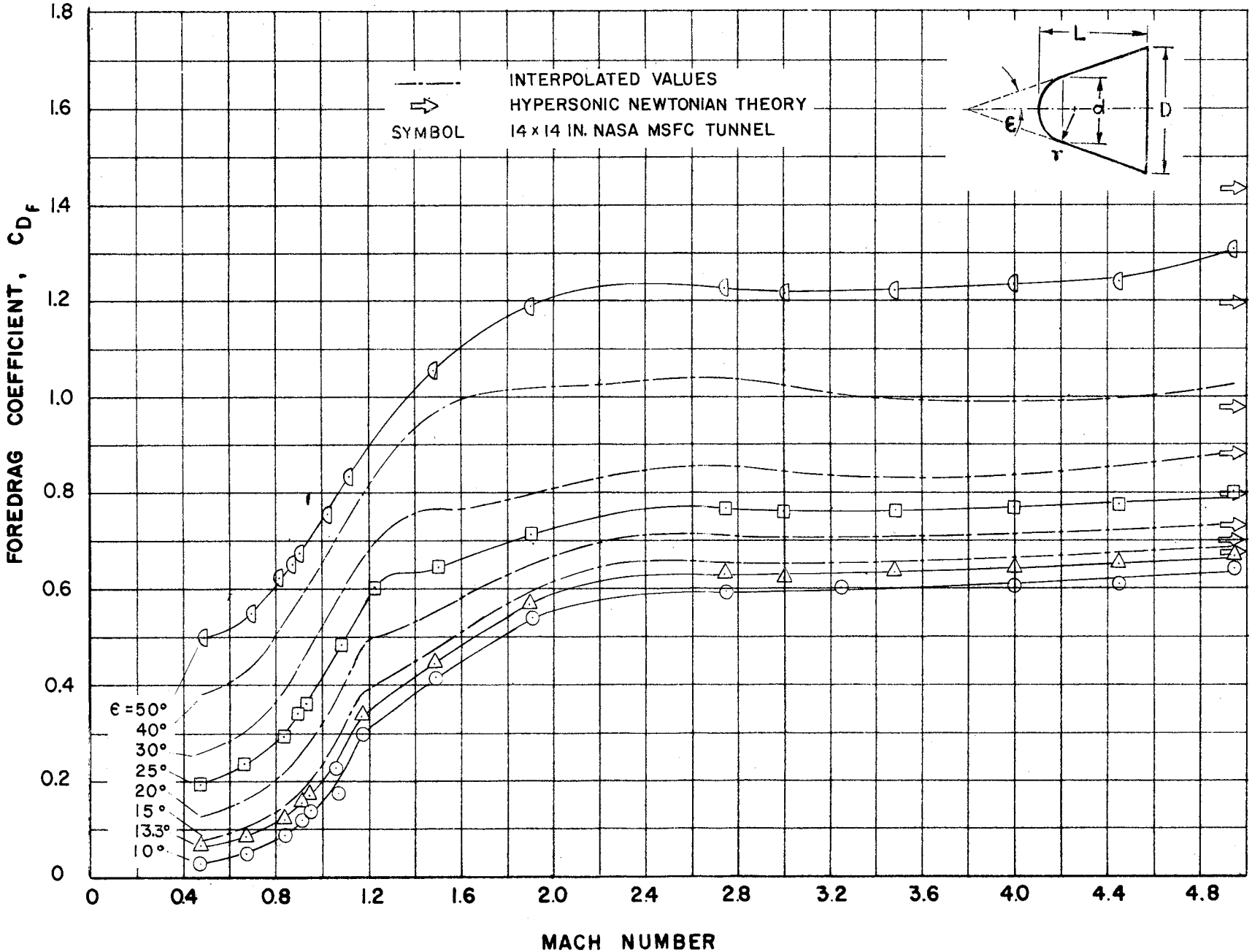

FIGURE 15. VARIATION OF FOREDRAG COEFFICIENT WITH MACH NUMBER FOR VARIOUS CONES (d/D = 0.8)

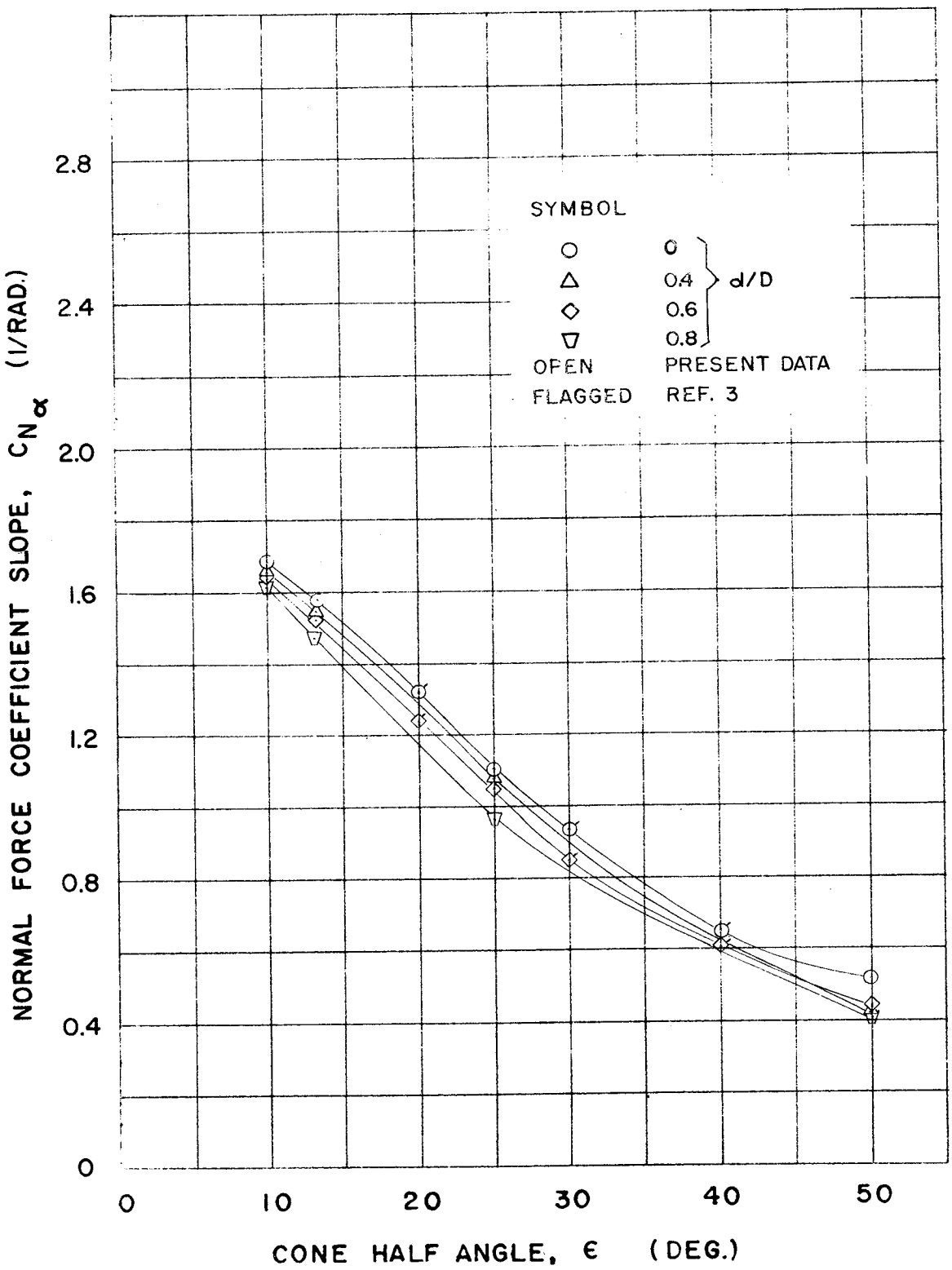

FIGURE 16. VARIATION OF NORMAL FORCE COEFFICIENT SLOPE WITH CONE HALF ANGLE AND BLUNTNESS AT M = 0.68

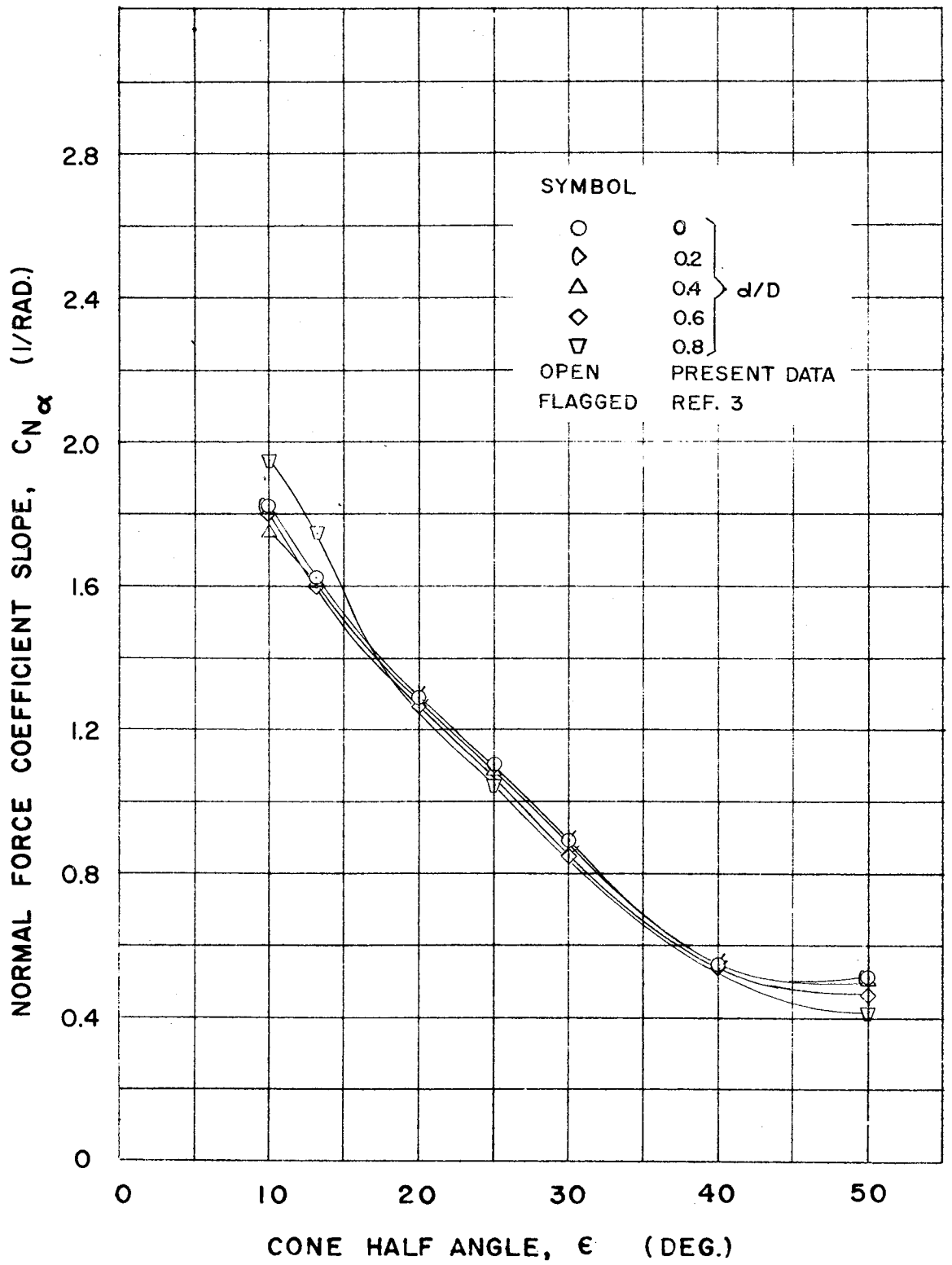

FIGURE 17. VARIATION OF NORMAL FORCE COEFFICIENT SLOPE WITH CONE HALF ANGLE AND BLUNTNESS AT M = 0.94

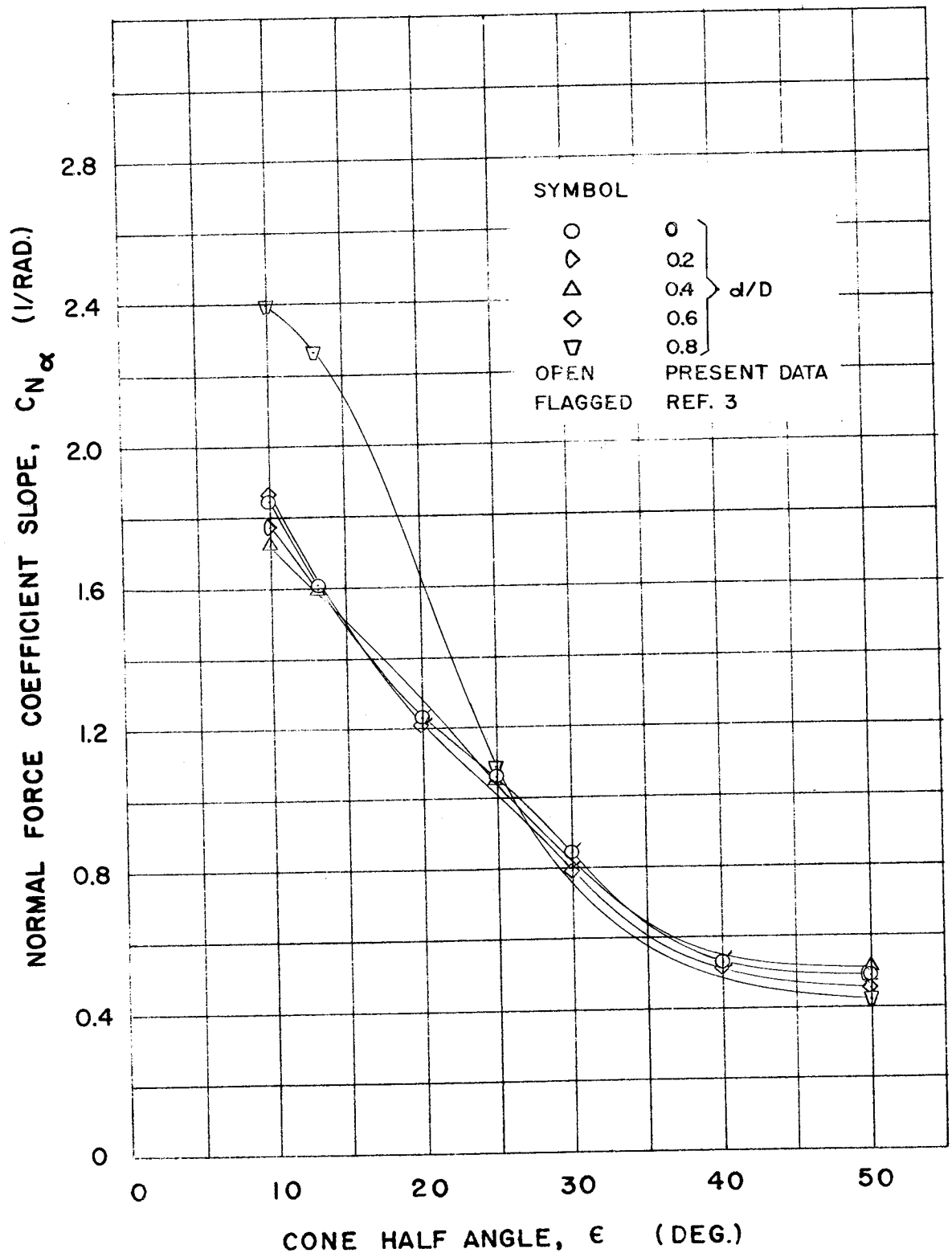

FIGURE 18. VARIATION OF NORMAL FORCE COEFFICIENT SLOPE WITH CONE HALF ANGLE AND BLUNTNESS AT M = 1.05

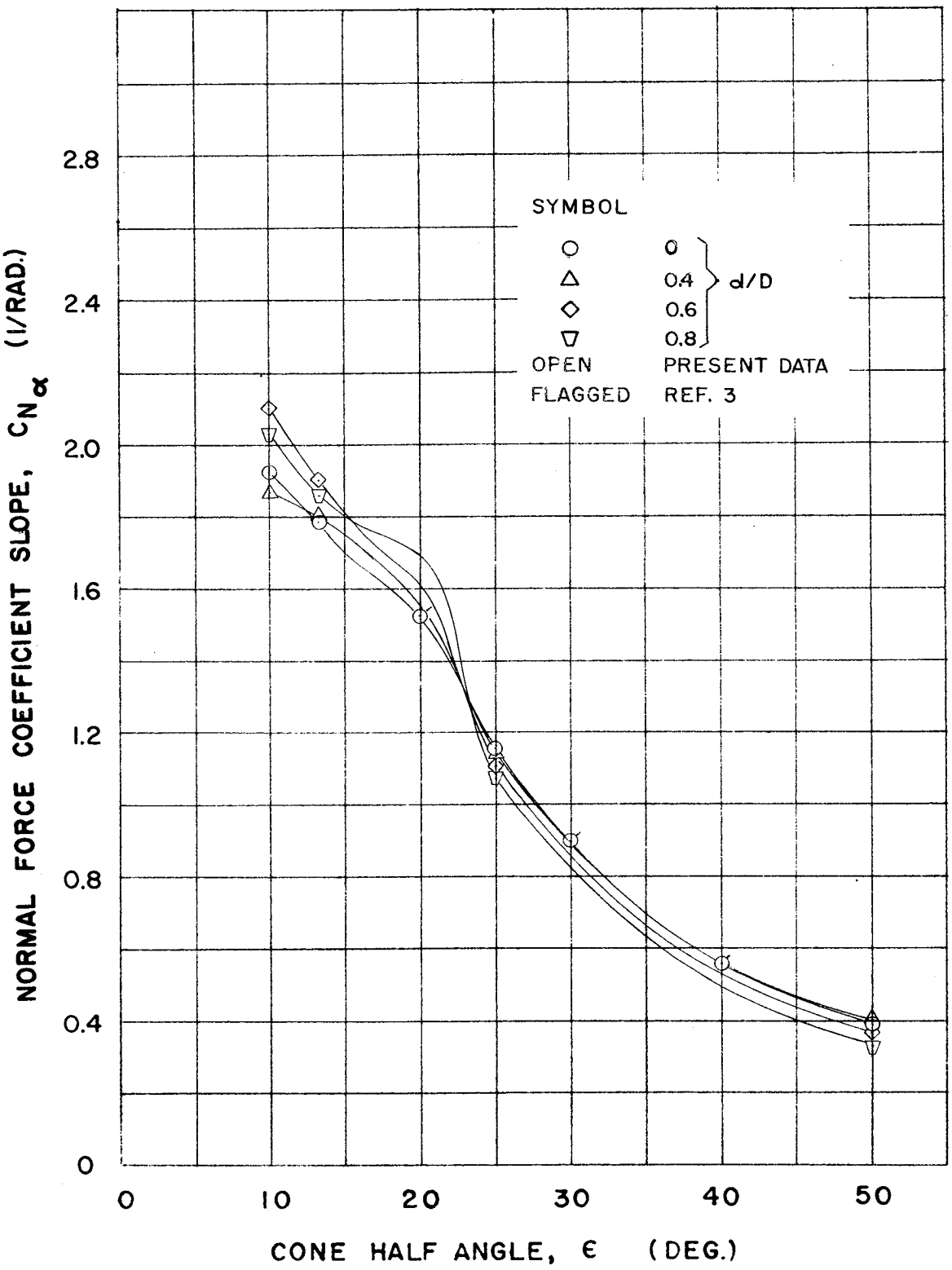

FIGURE 19. VARIATION OF NORMAL FORCE COEFFICIENT SLOPE WITH CONE HALF ANGLE AND BLUNTNESS AT M = 1.30

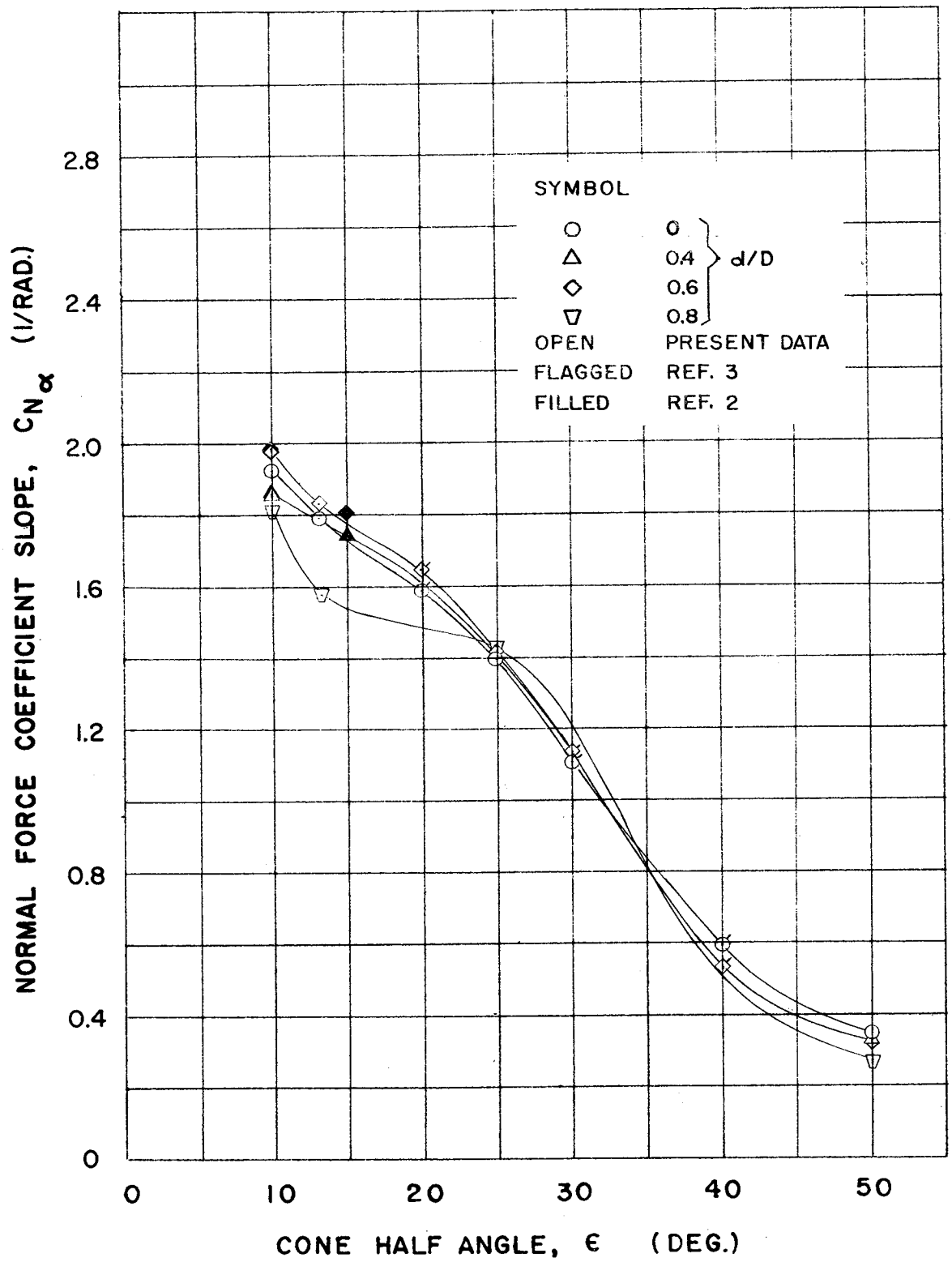

FIGURE 20. VARIATION OF NORMAL FORCE COEFFICIENT SLOPE WITH CONE HALF ANGLE AND BLUNTNESS AT M = 1.50

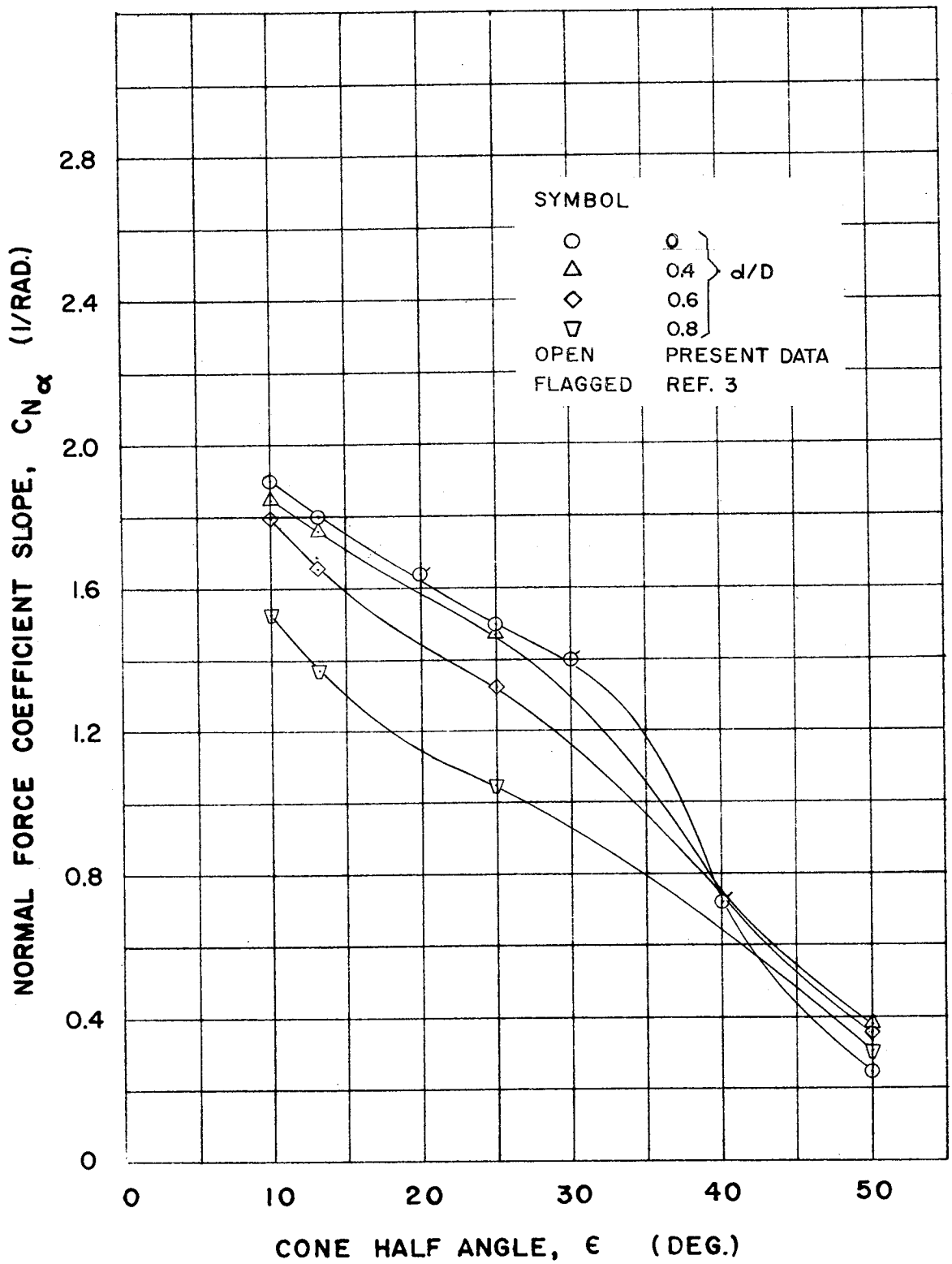

FIGURE 21. VARIATION OF NORMAL FORCE COEFFICIENT SLOPE WITH CONE HALF ANGLE AND BLUNTNESS AT M = 1.97

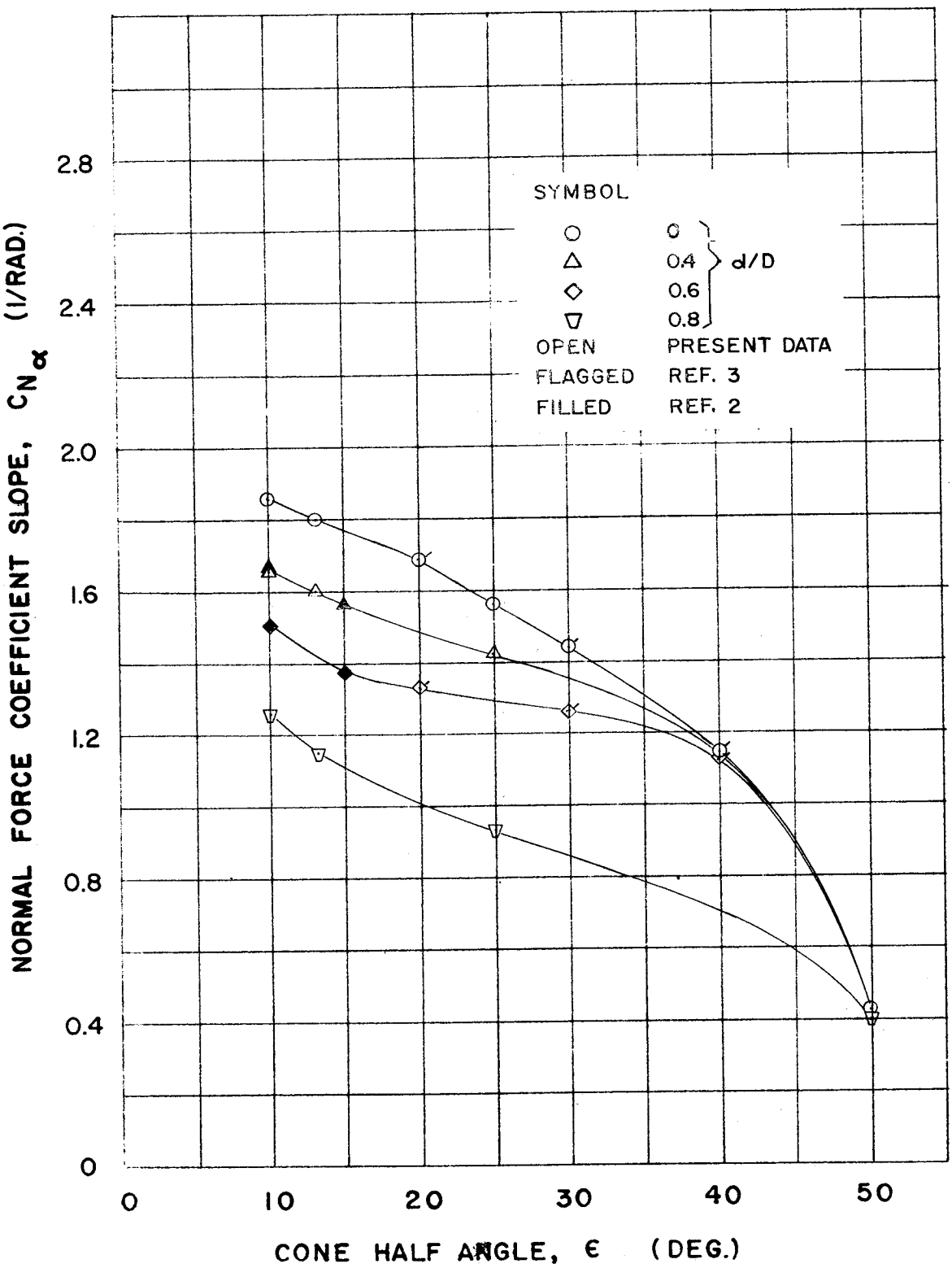

FIGURE 22. VARIATION OF NORMAL FORCE COEFFICIENT SLOPE WITH CONE HALF ANGLE AND BLUNTNESS AT M = 2.75

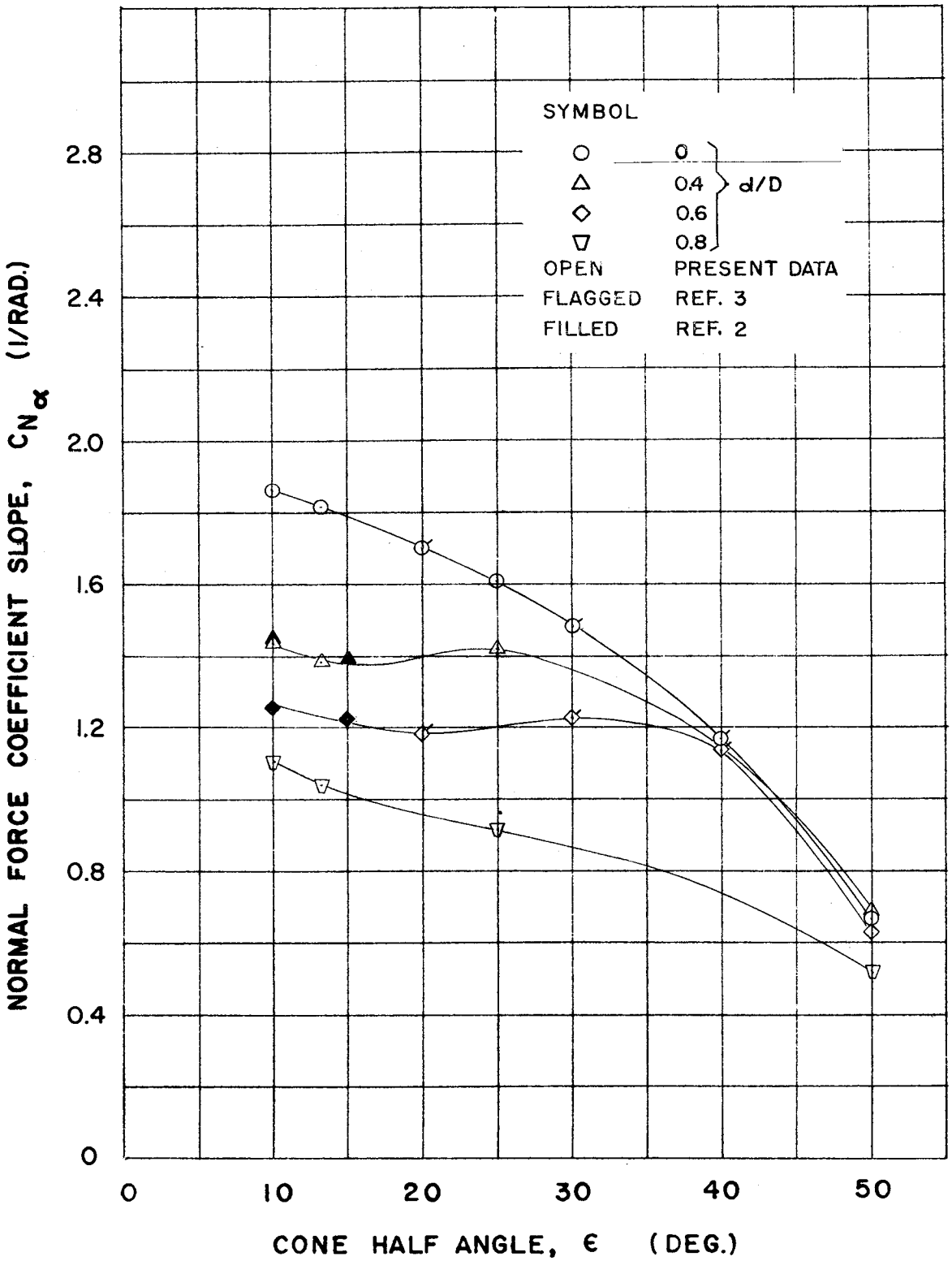

FIGURE 23. VARIATION OF NORMAL FORCE COEFFICIENT SLOPE WITH CONE HALF ANGLES AND BLUNTNESS AT M = 4.00

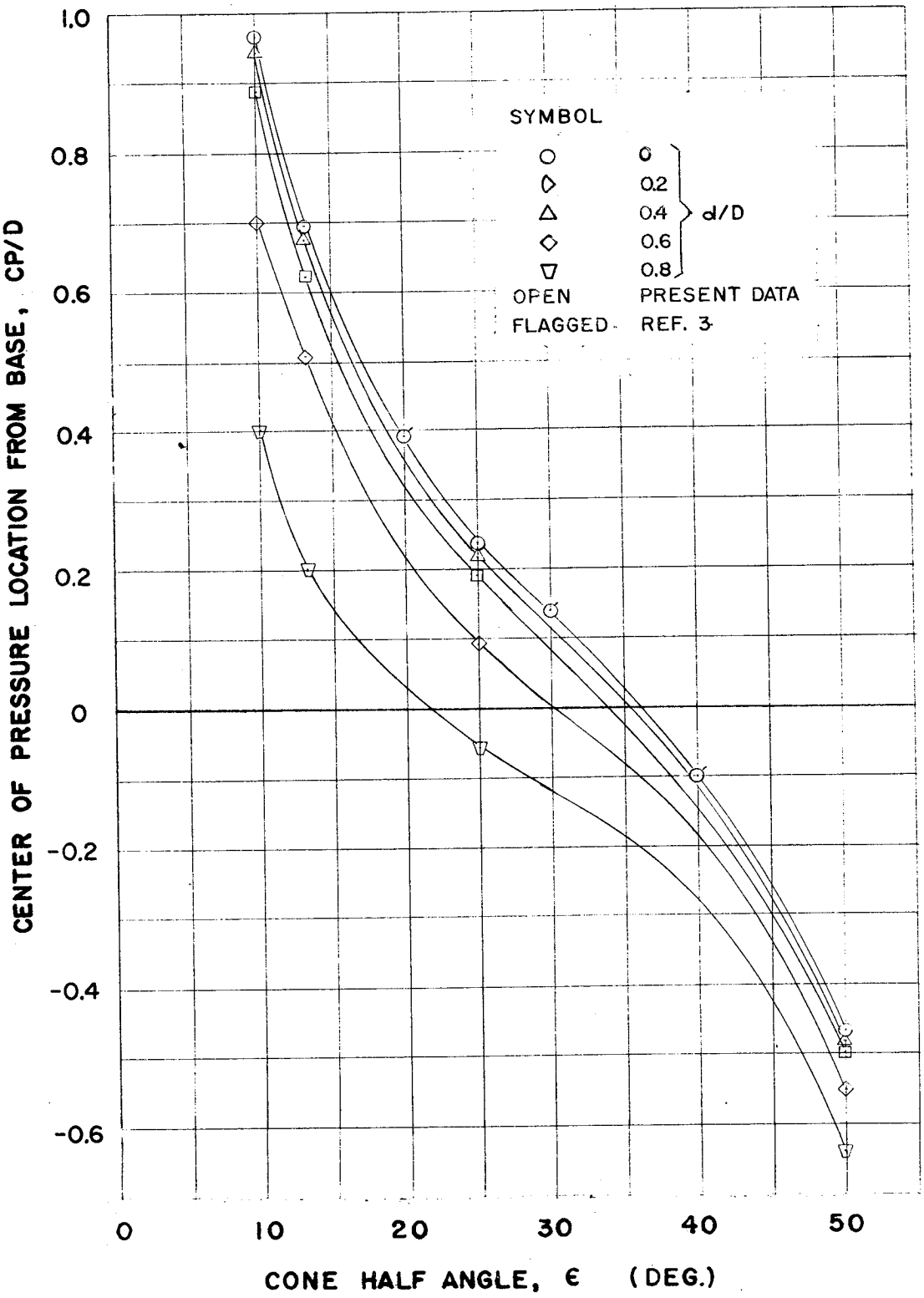

FIGURE 24. VARIATION OF CENTER OF PRESSURE WITH CONE HALF ANGLE AND BLUNTNESS AT M = 0.68

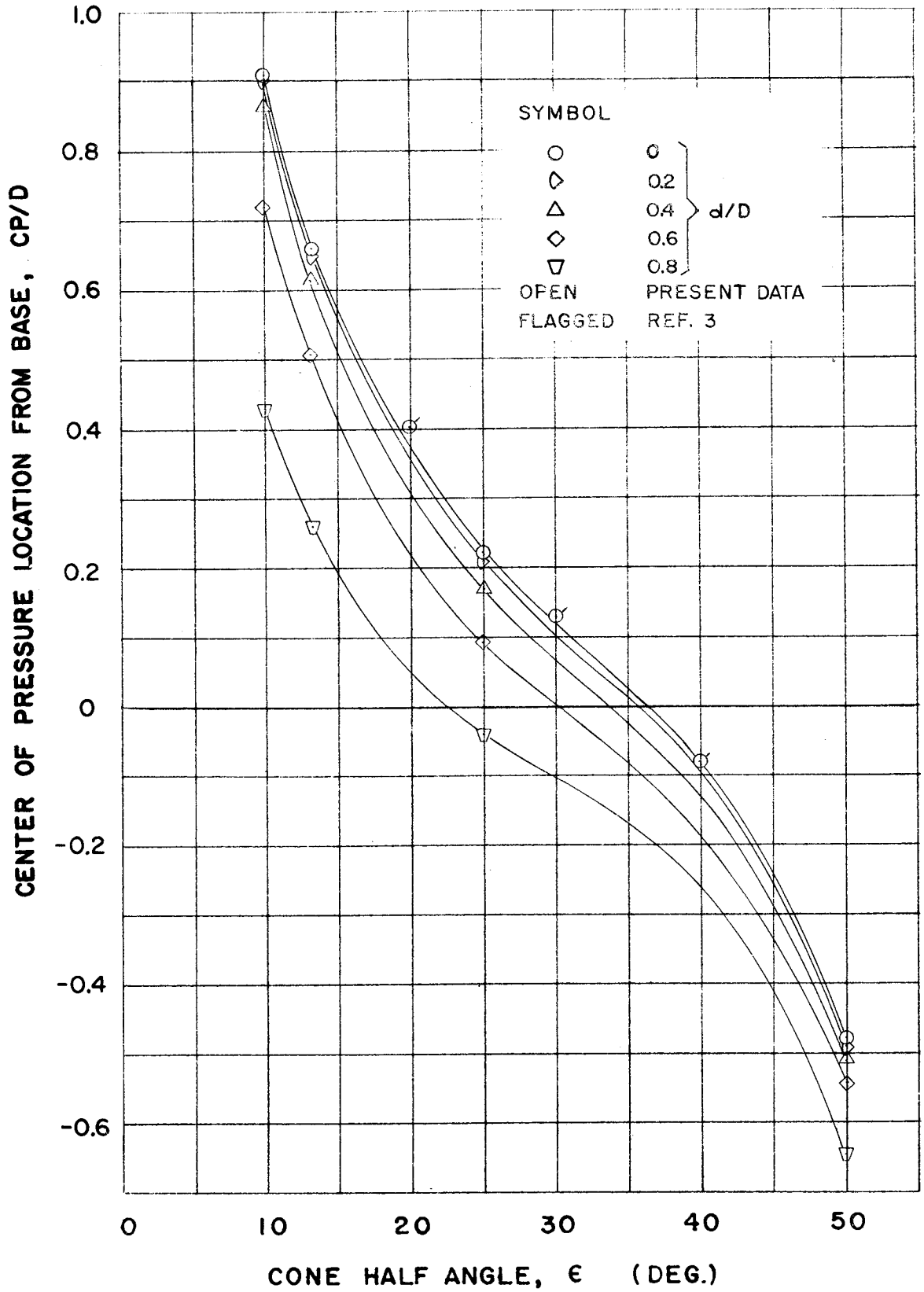

FIGURE 25. VARIATION OF CENTER OF PRESSURE WITH CONE HALF ANGLE AND BLUNTNESS AT M = 0.94

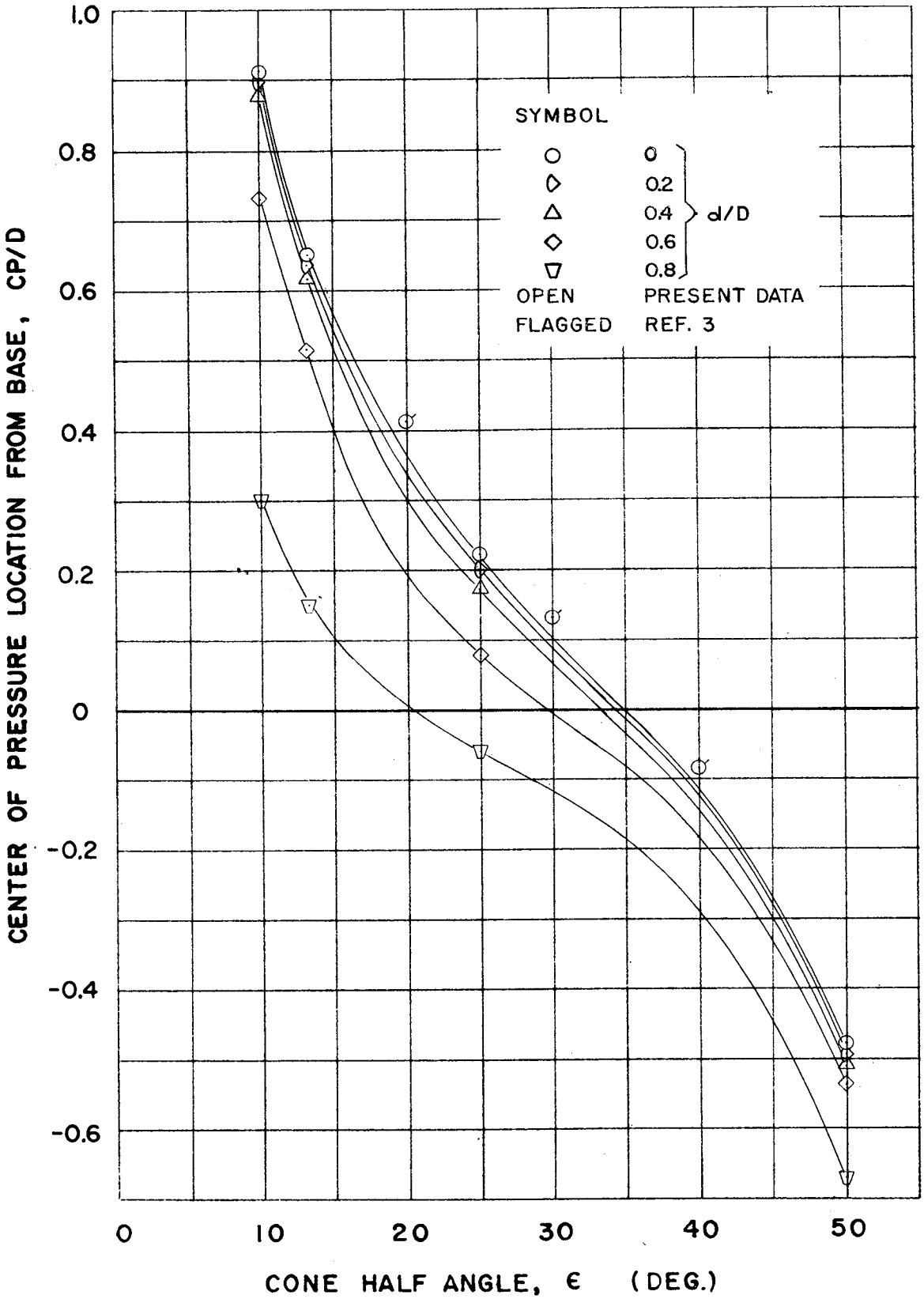

FIGURE 26. VARIATION OF CENTER OF PRESSURE WITH CONE HALF ANGLE AND BLUNTNESS AT M = 1.05

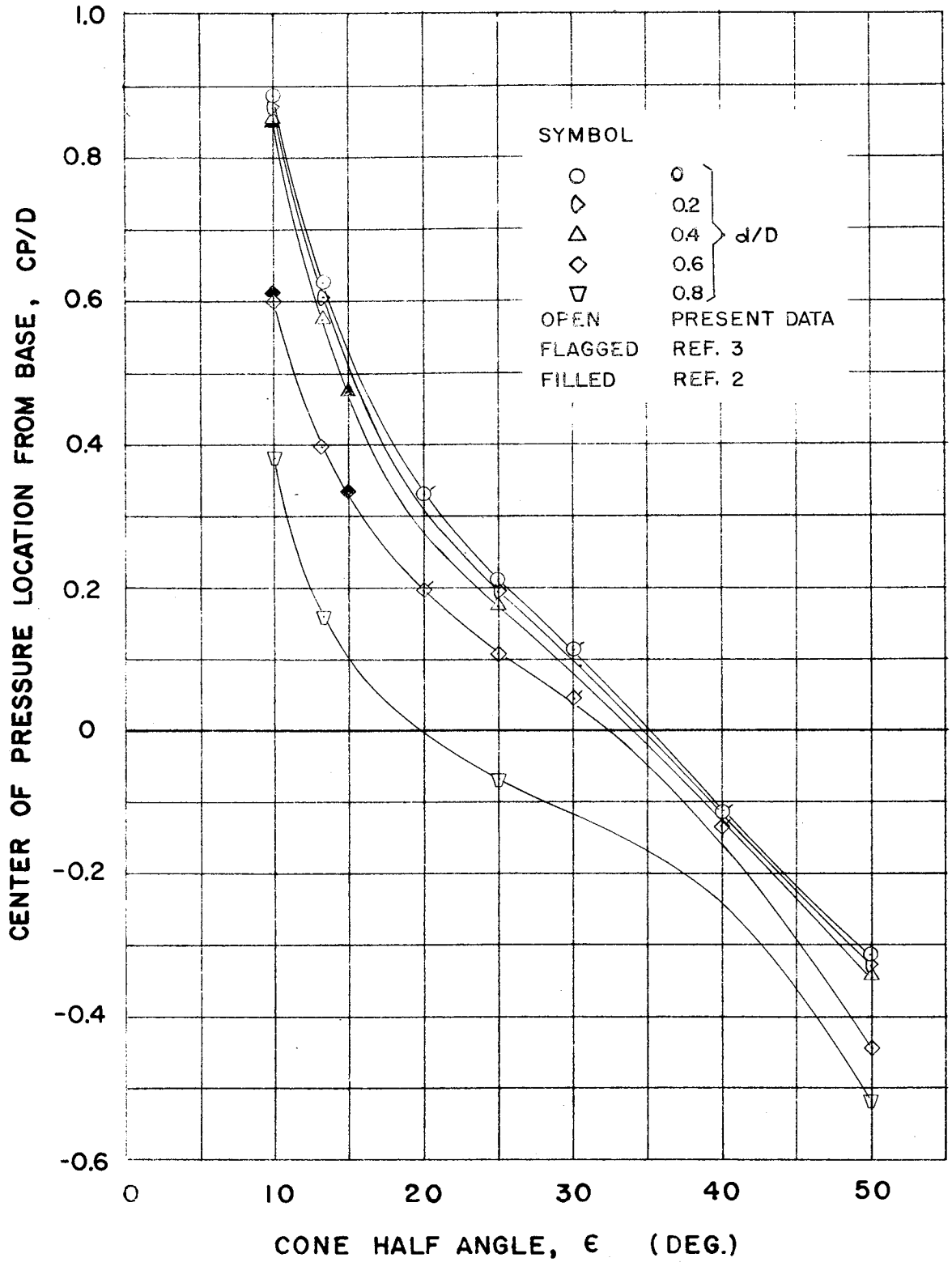

FIGURE 27. VARIATION OF CENTER OF PRESSURE WITH CONE HALF ANGLE AND BLUNTNESS AT M = 1.50

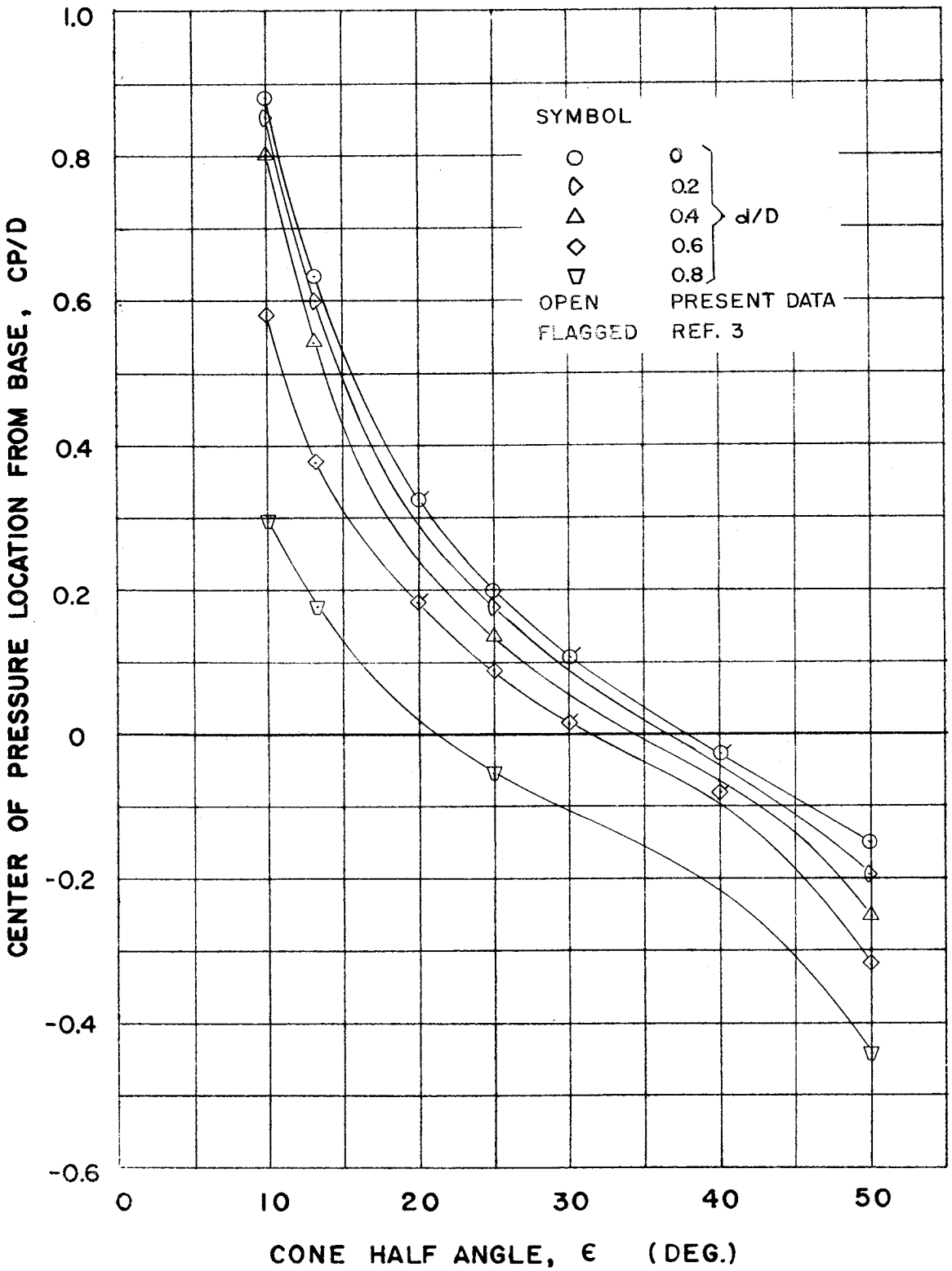

FIGURE 28. VARIATION OF CENTER OF PRESSURE WITH CONE HALF ANGLE AND BLUNTNESS AT M = 1.97

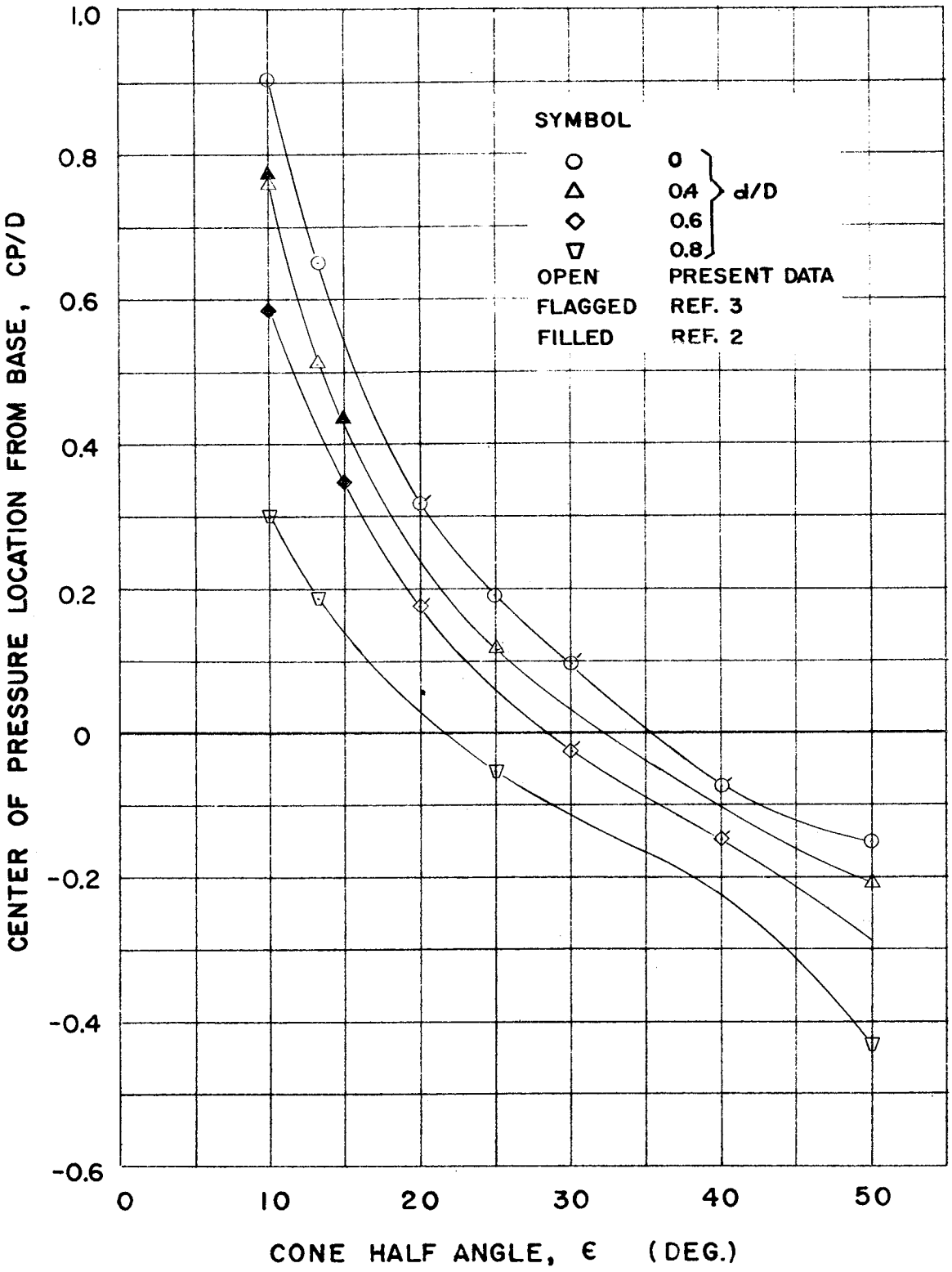

FIGURE 29. VARIATION OF CENTER OF PRESSURE WITH CONE HALF ANGLE AND BLUNTNESS AT M = 2.75

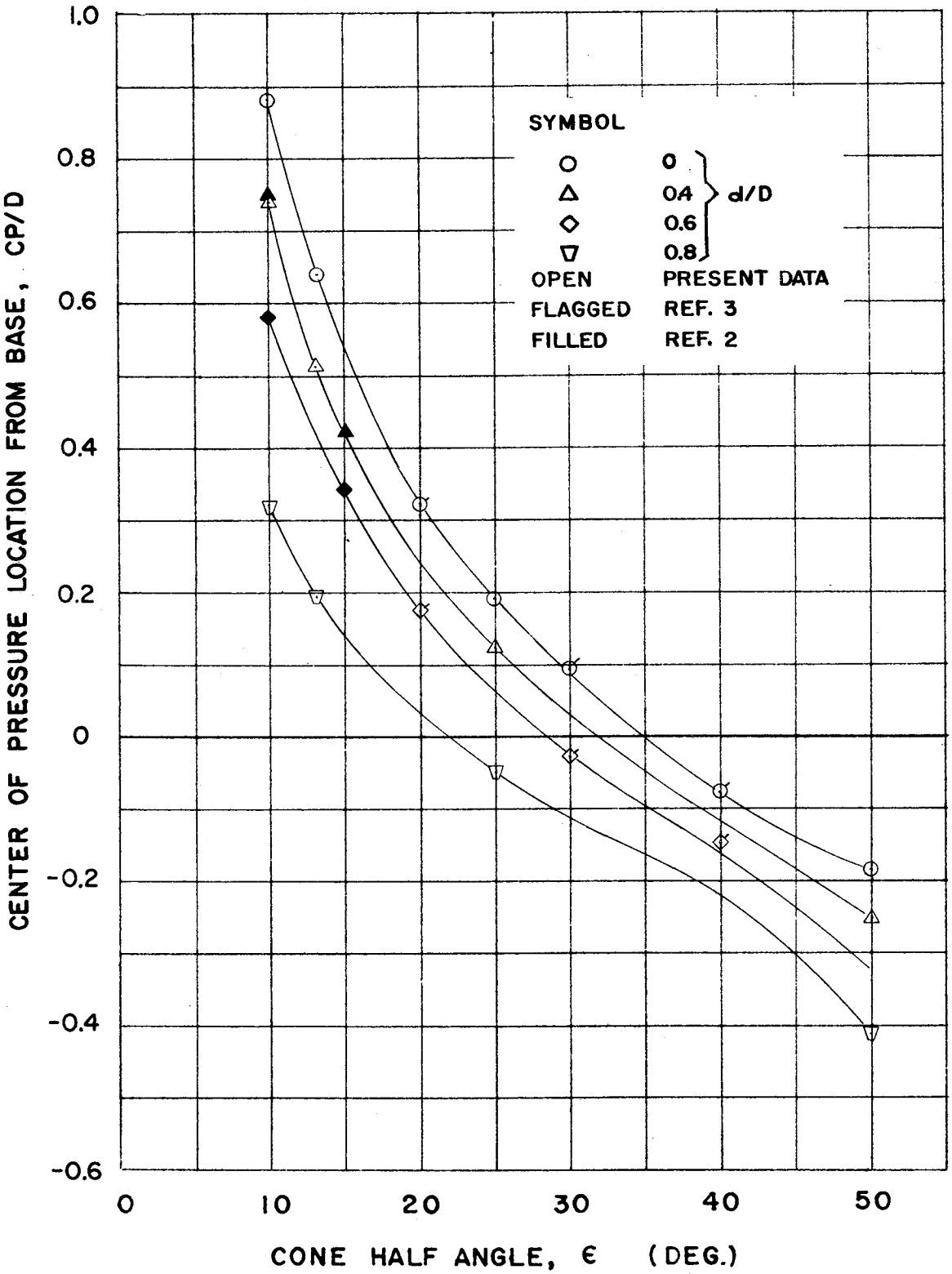

FIGURE 30. VARIATION OF CENTER OF PRESSURE WITH CONE HALF ANGLE AND BLUNTNESS AT M = 4.00

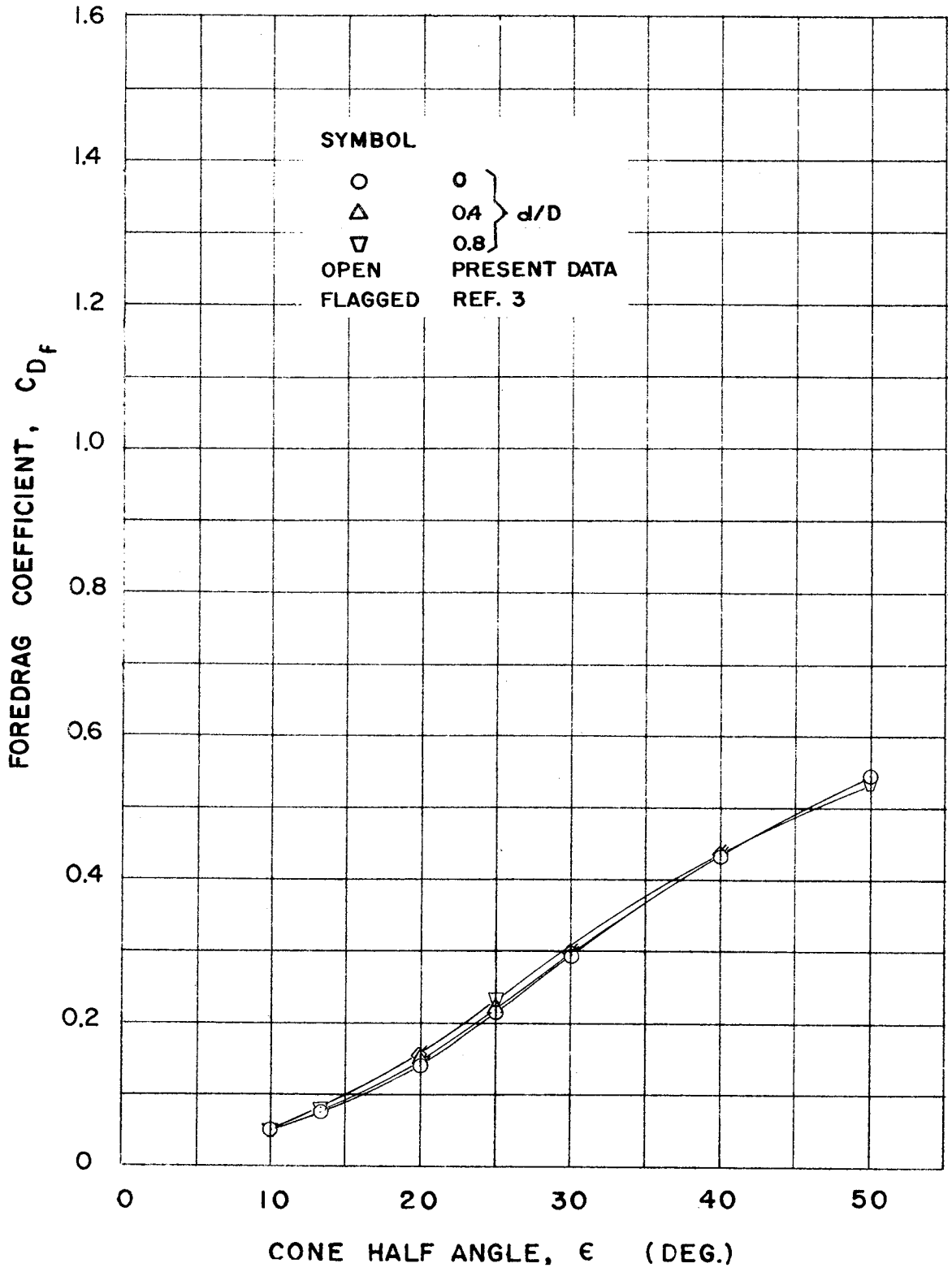

FIGURE 31. VARIATION OF FOREDRAG COEFFICIENT WITH CONE HALF ANGLE AND BLUNTNESS AT M = 0.68

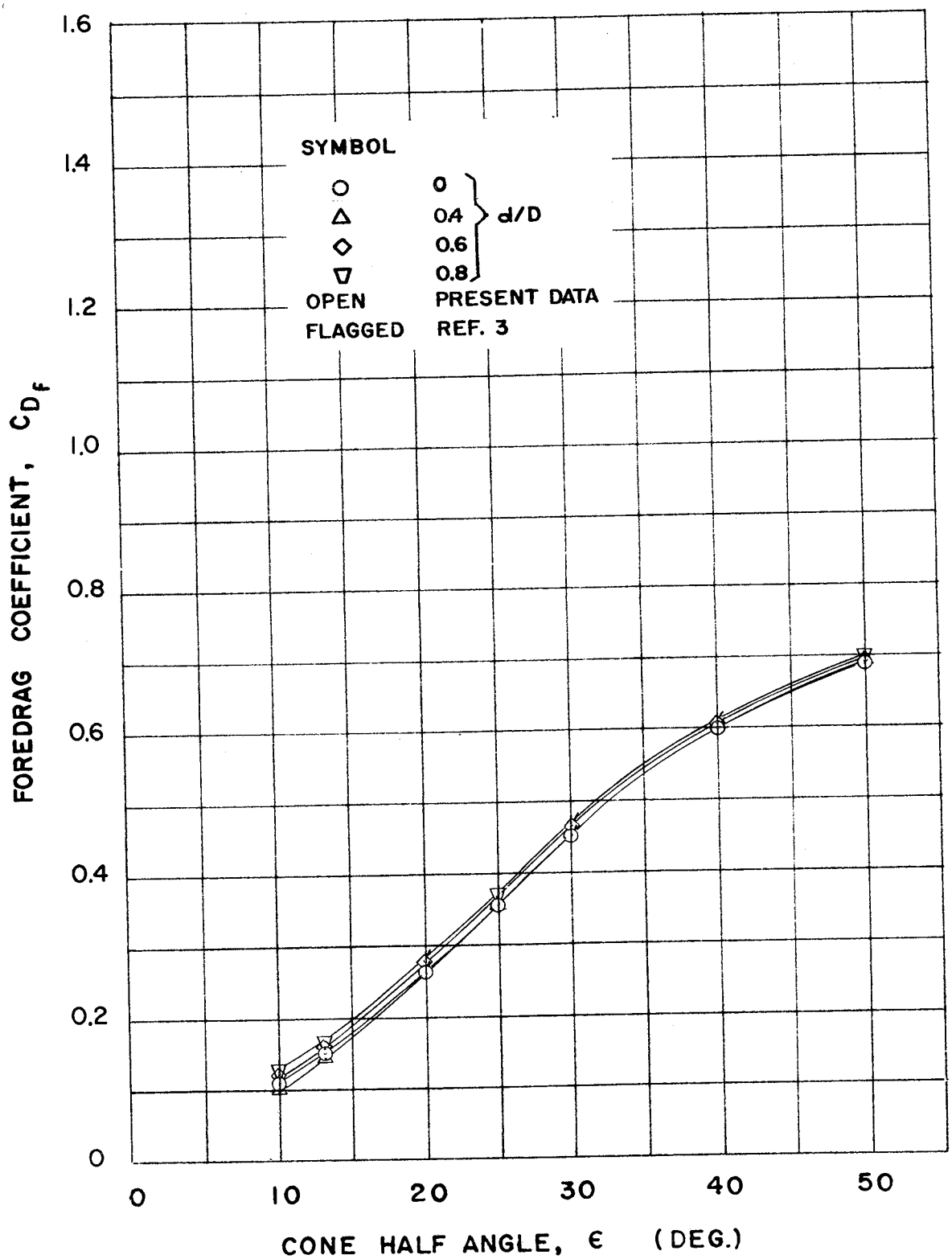

FIGURE 32. VARIATION OF FOREDRAG COEFFICIENT WITH CONE HALF ANGLE AND BLUNTNESS AT M = 0.94

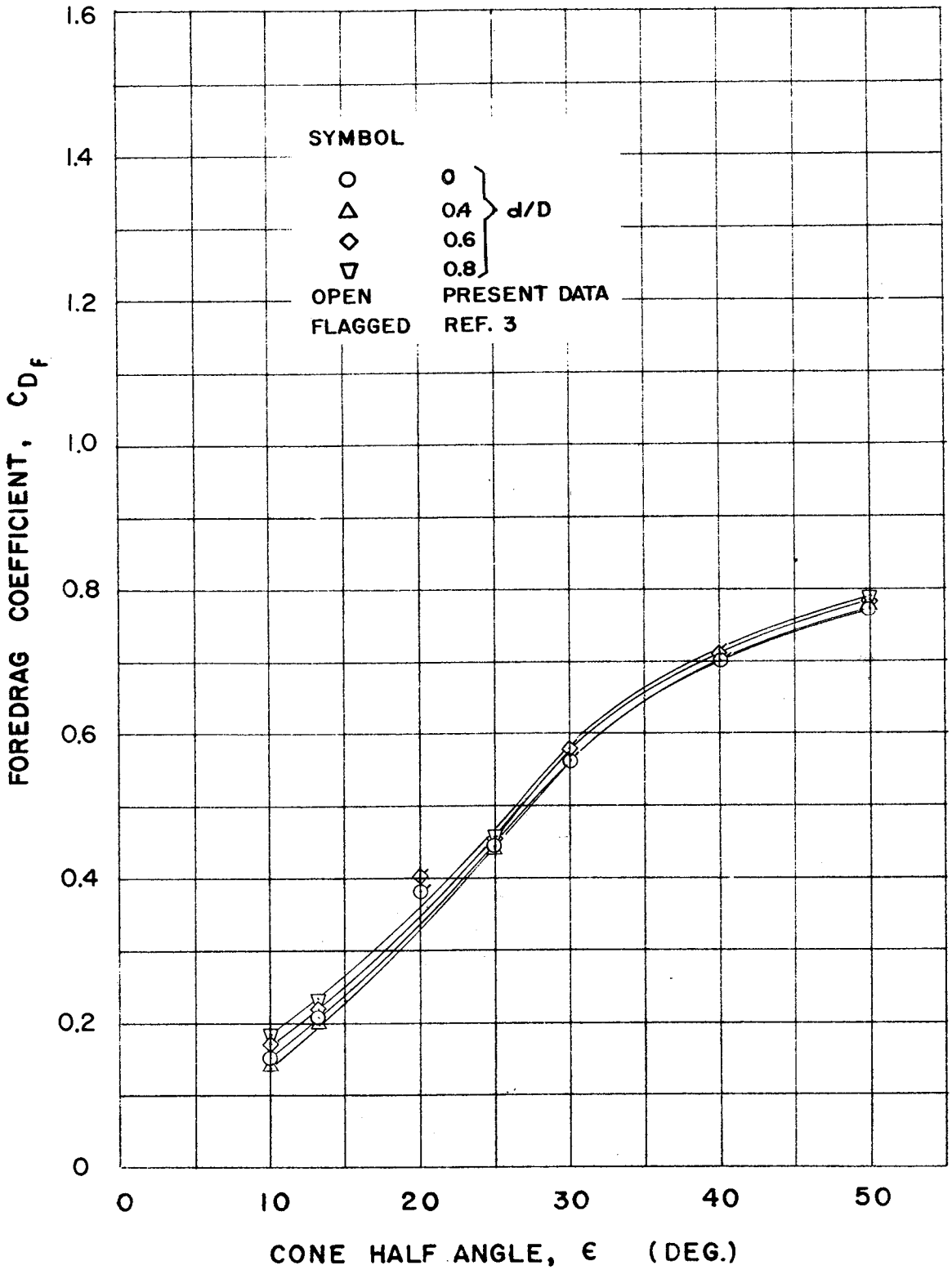

FIGURE 33. VARIATION OF FOREDRAG COEFFICIENT WITH CONE HALF ANGLE AND BLUNTNESS AT M = 1.05

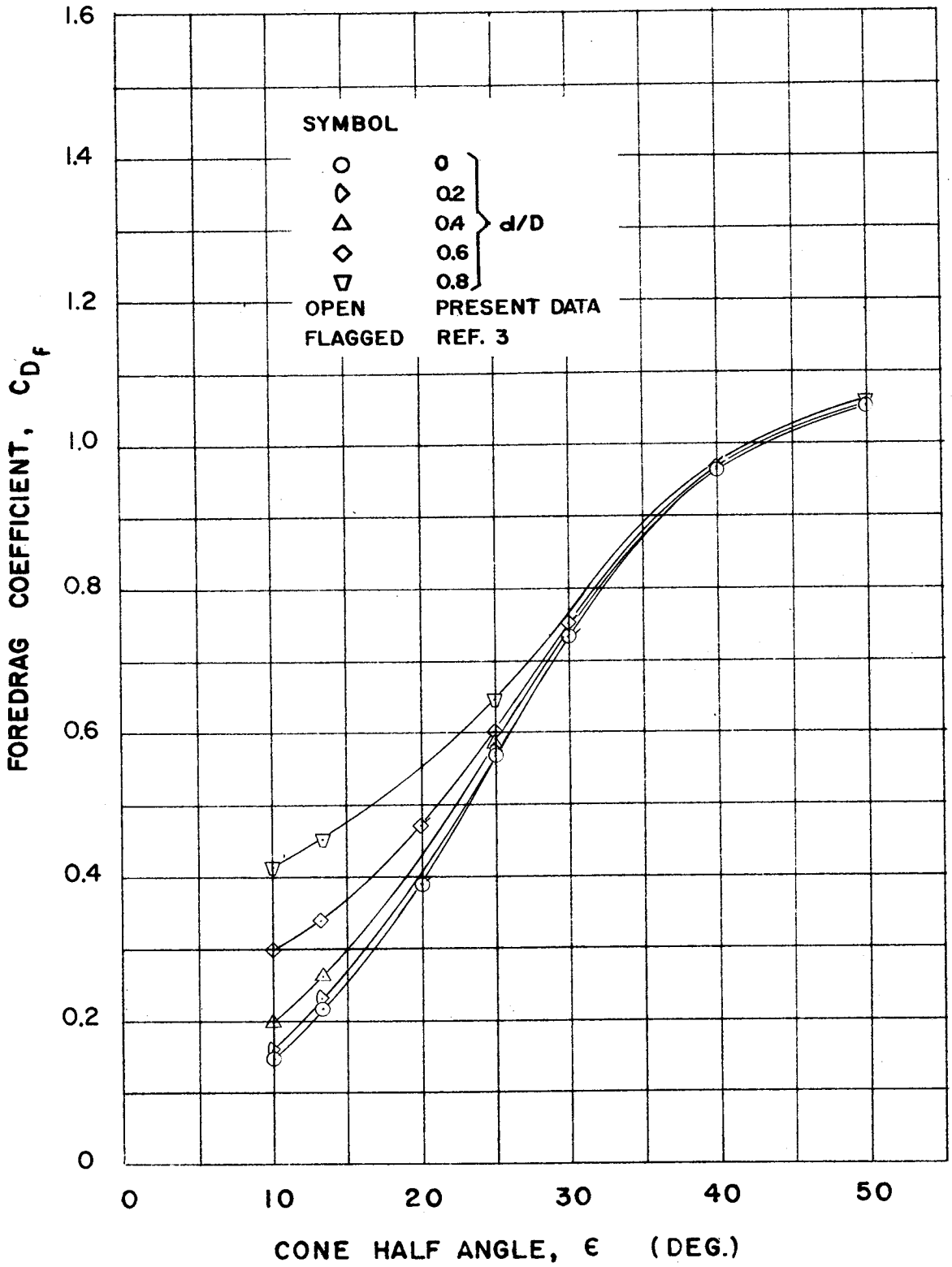

FIGURE 34. VARIATION OF FOREDRAG COEFFICIENT WITH CONE HALF ANGLE AND BLUNTNESS AT M = 1.50

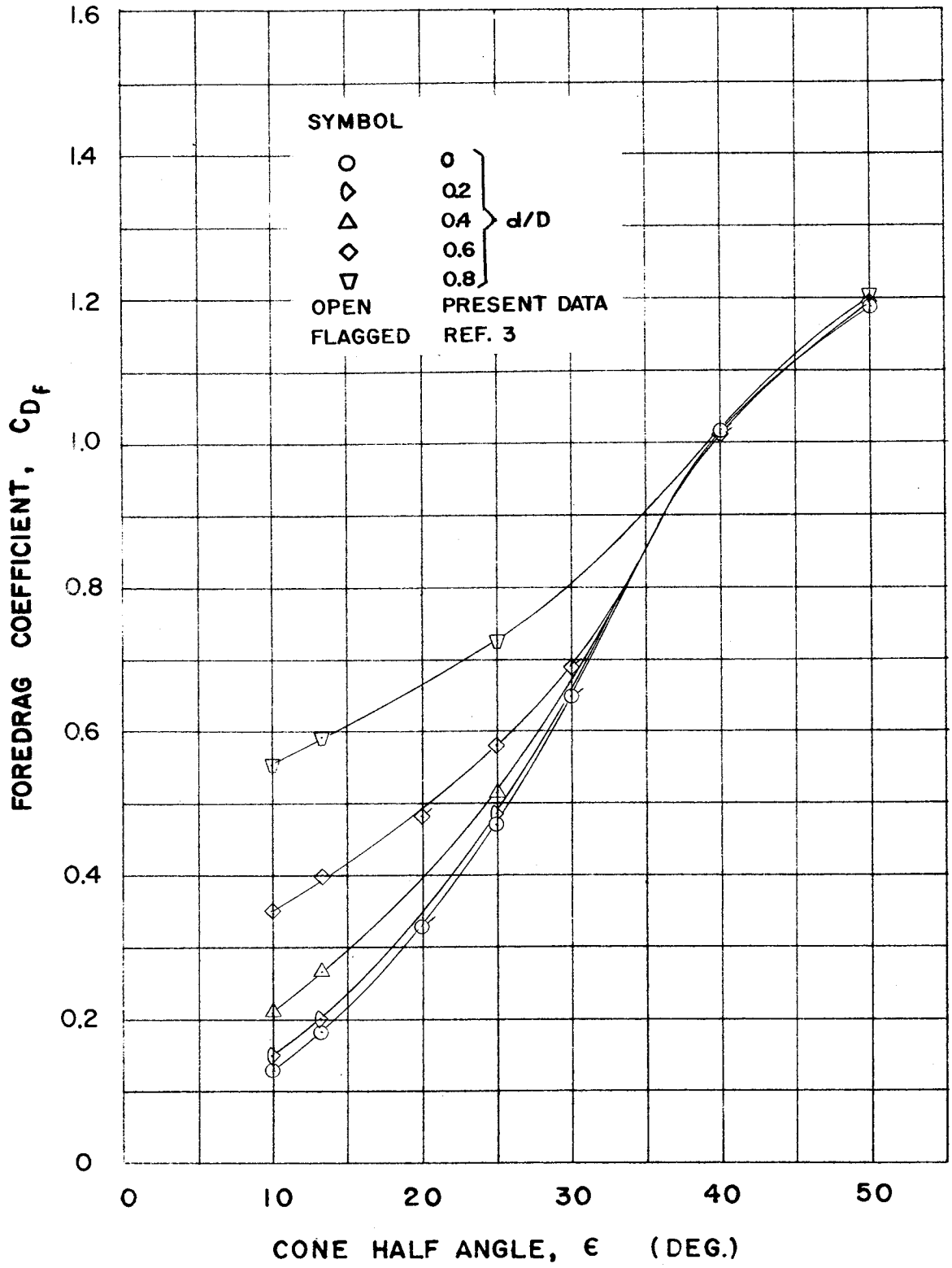

FIGURE 35. VARIATION OF FOREDRAG COEFFICIENT WITH CONE HALF ANGLE AND BLUNTNESS AT M = 1.97

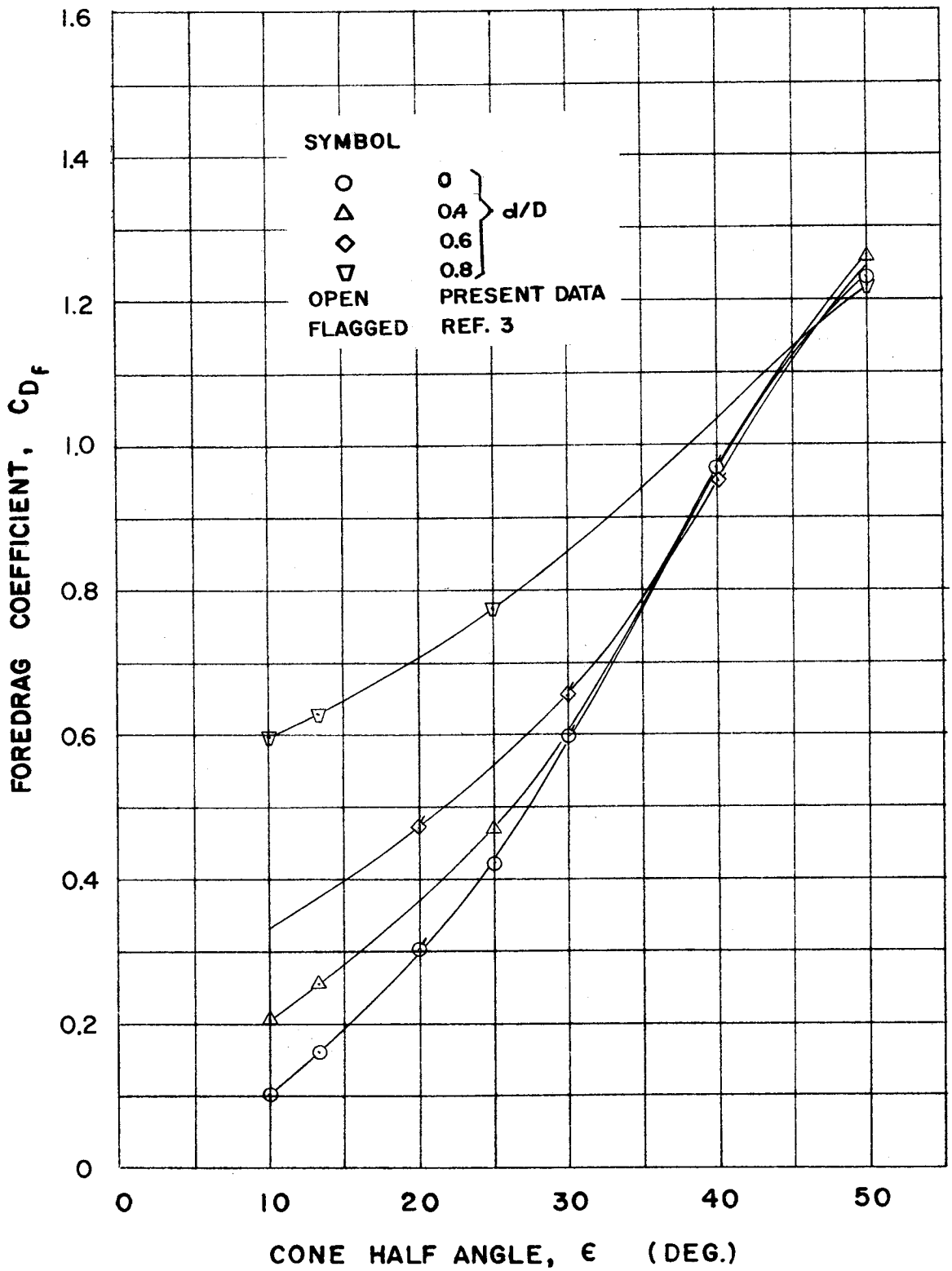

FIGURE 36. VARIATION OF FOREDRAG COEFFICIENT WITH CONE HALF ANGLE AND BLUNTNESS AT M = 2.75

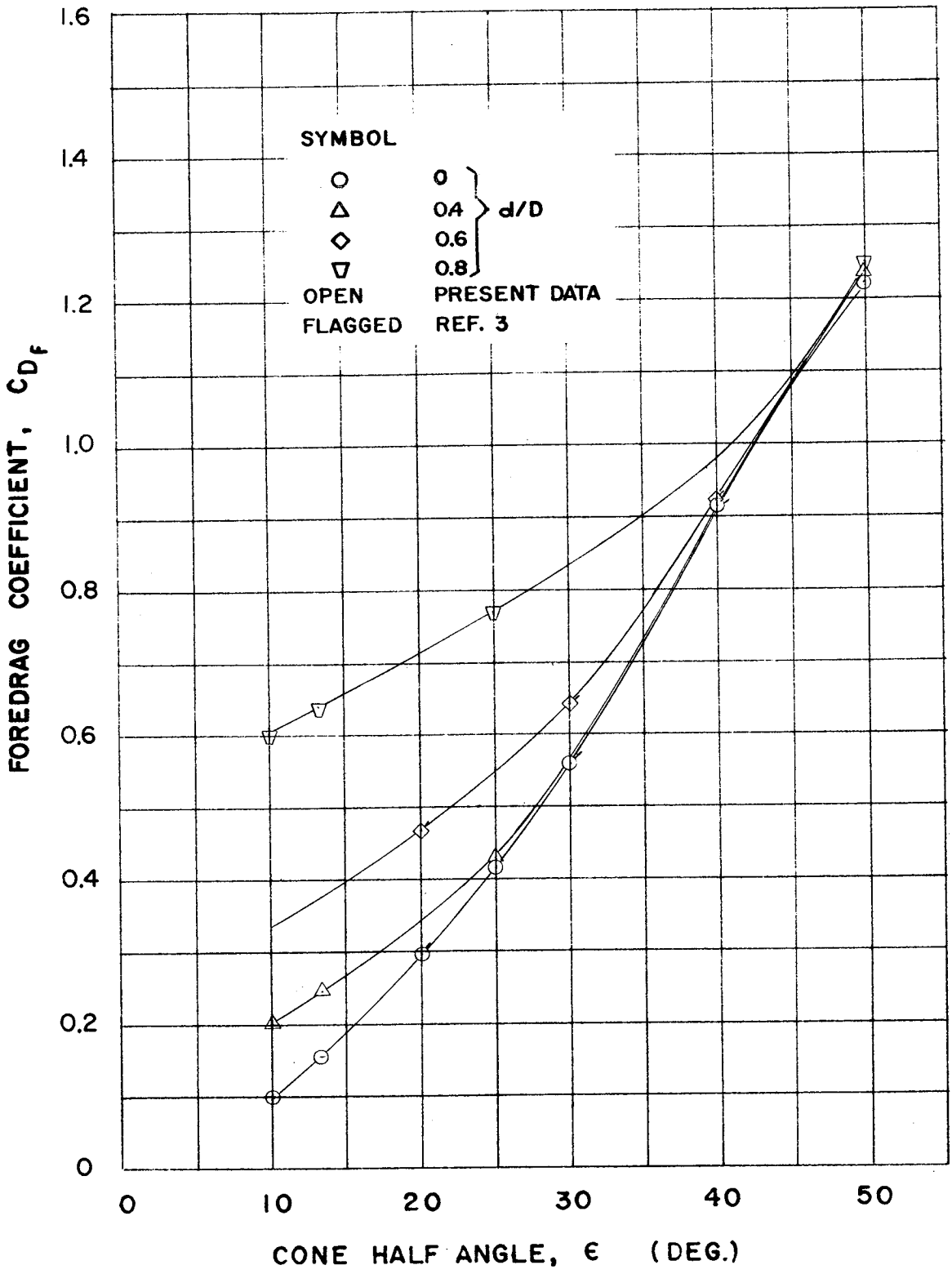

FIGURE 37. VARIATION OF FOREDRAG COEFFICIENT WITH CONE HALF ANGLE AND BLUNTNESS AT M = 4.00

APPENDIX

To allow quick estimation of the basic aerodynamic characteristics by the Hypersonic Newtonian Impact Theory (Ref. 6), the necessary relationships of cone geometry parameters are presented in Figures A-1 and A-2. The charts of theoretical normal force coefficient slopes, center of pressure locations, and wave drag coefficients are given in Figures A-3 through A-5

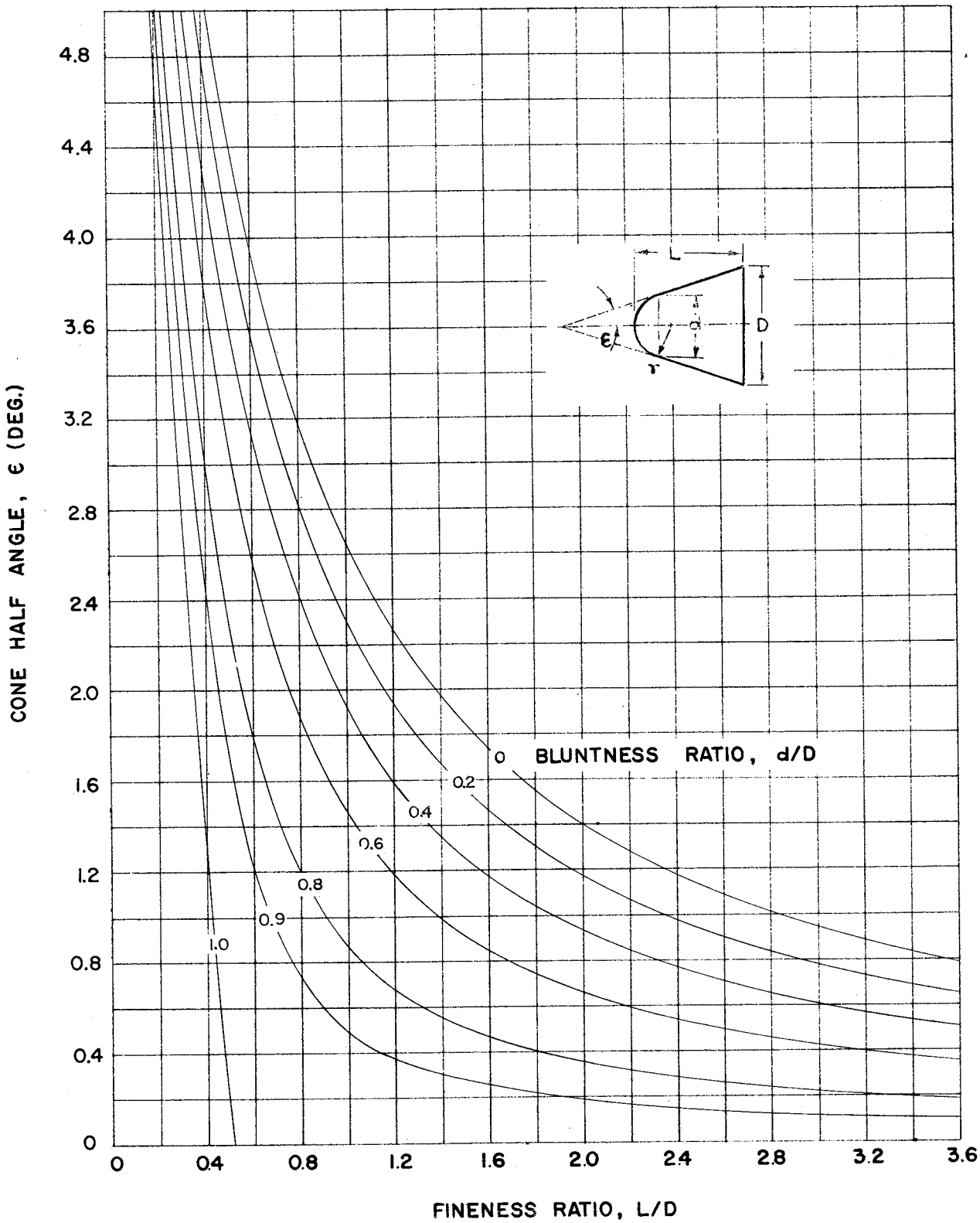

FIGURE A-1. RELATIONSHIP BETWEEN GEOMETRIC PARAMETERS OF SPHERICALLY BLUNTED CONES

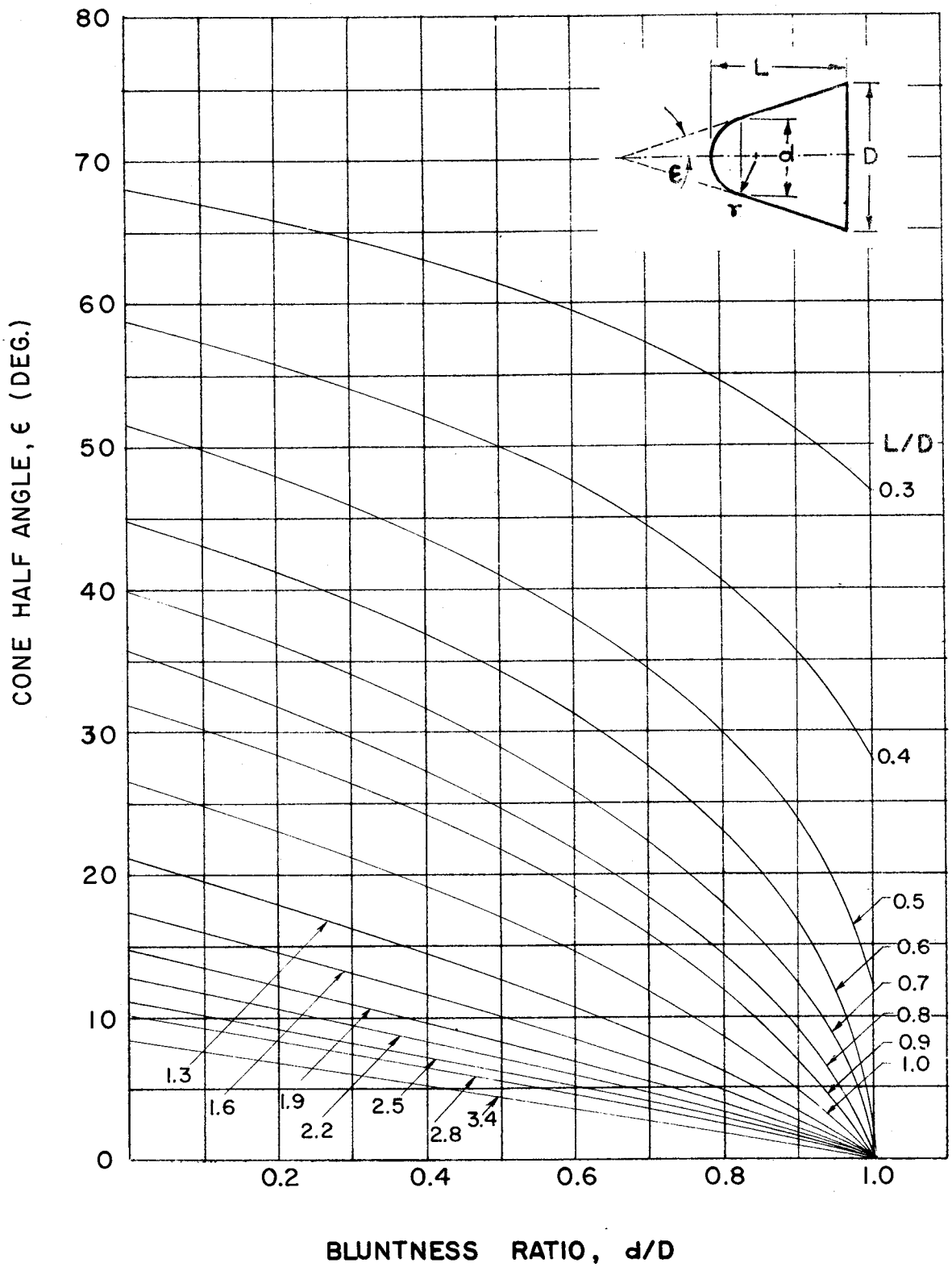

FIGURE A-2. RELATIONSHIP BETWEEN GEOMETRIC PARAMETERS OF SPHERICALLY BLUNTED CONES

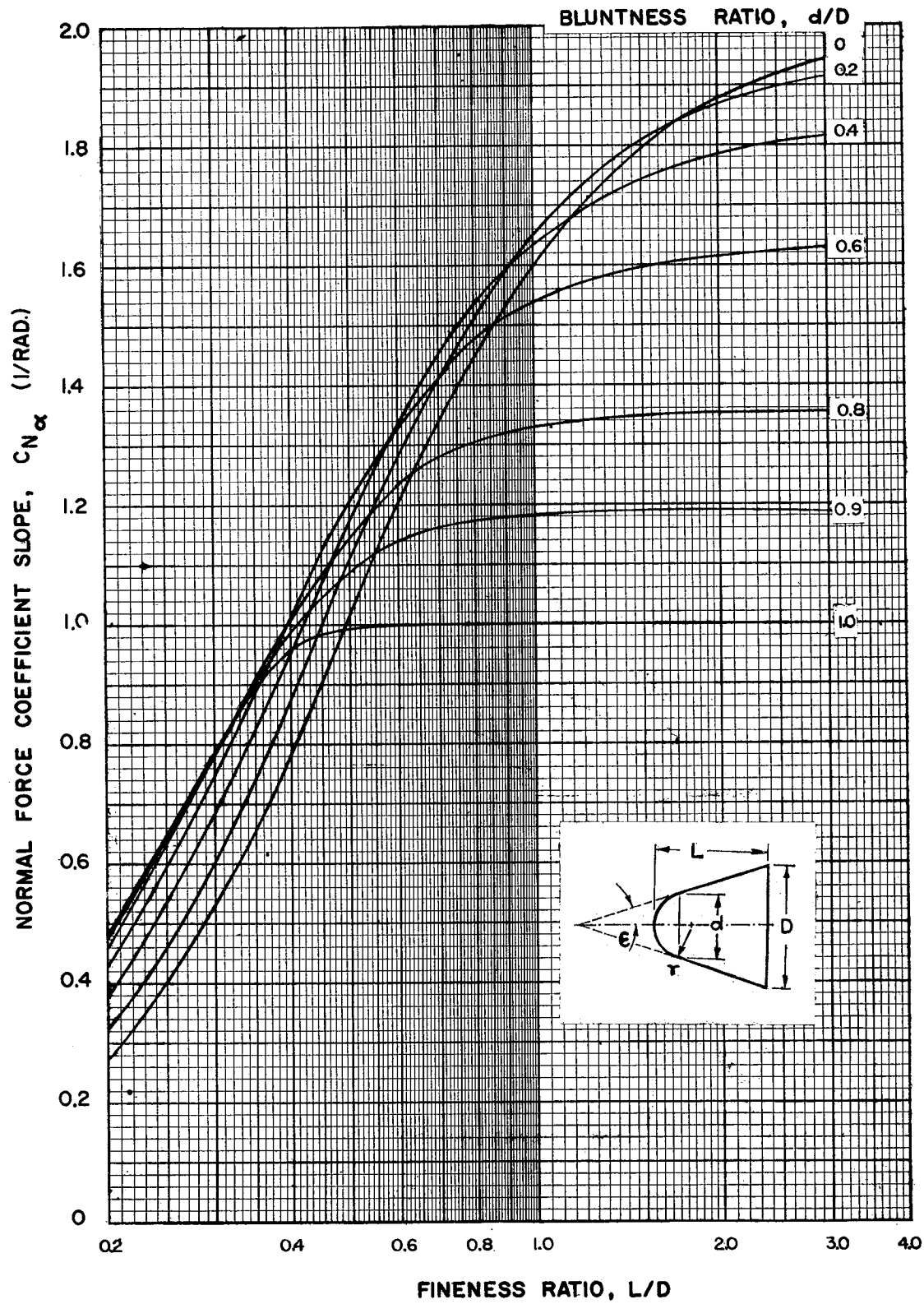

FIGURE A-3. HYPERSONIC NEWTONIAN NORMAL FORCE COEFFICIENT SLOPE FOR CONES OF VARYING GEOMETRY

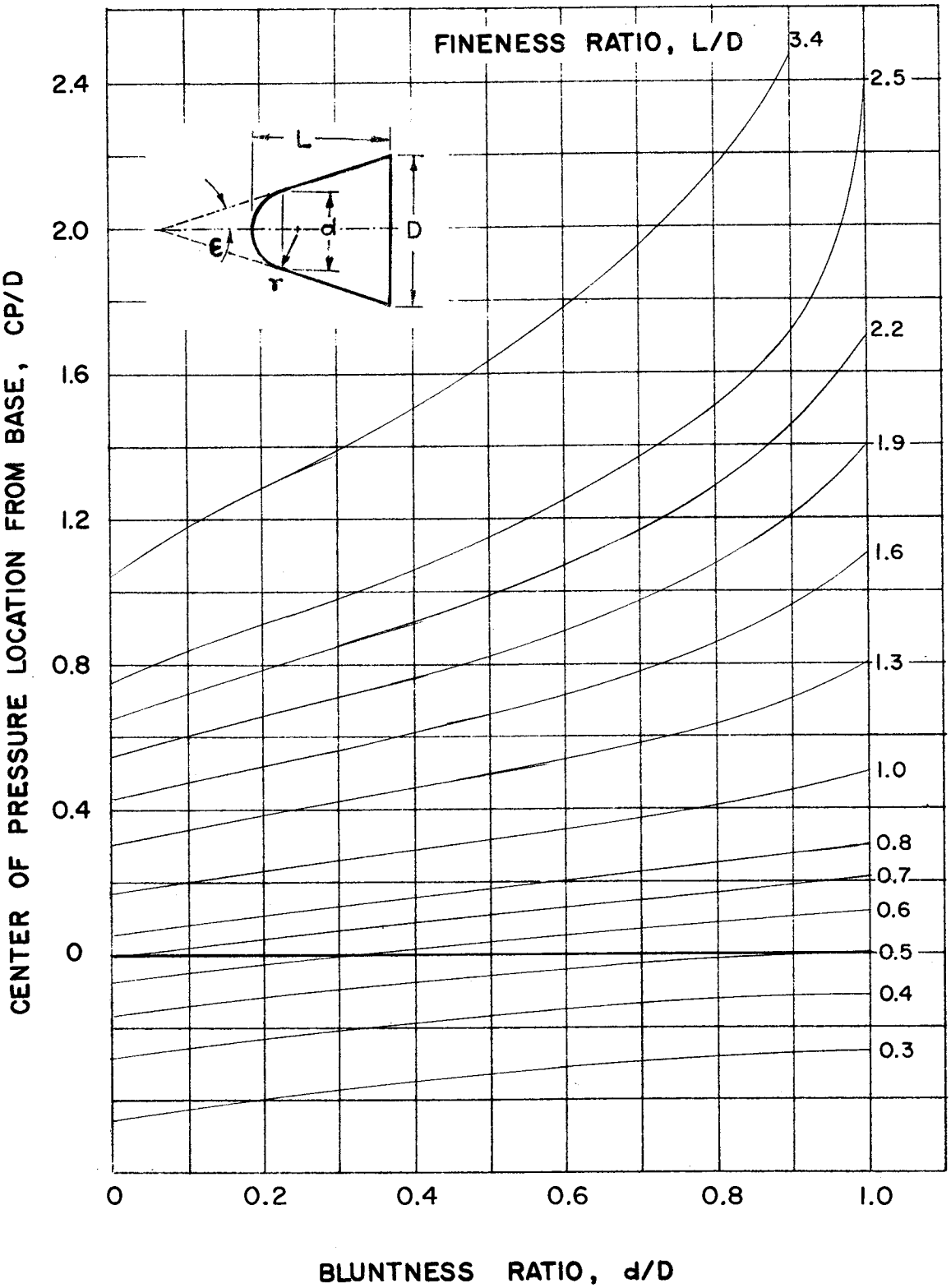

FIGURE A-4. HYPERSONIC NEWTONIAN CENTERS OF PRESSURE FOR CONES OF VARYING GEOMETRY

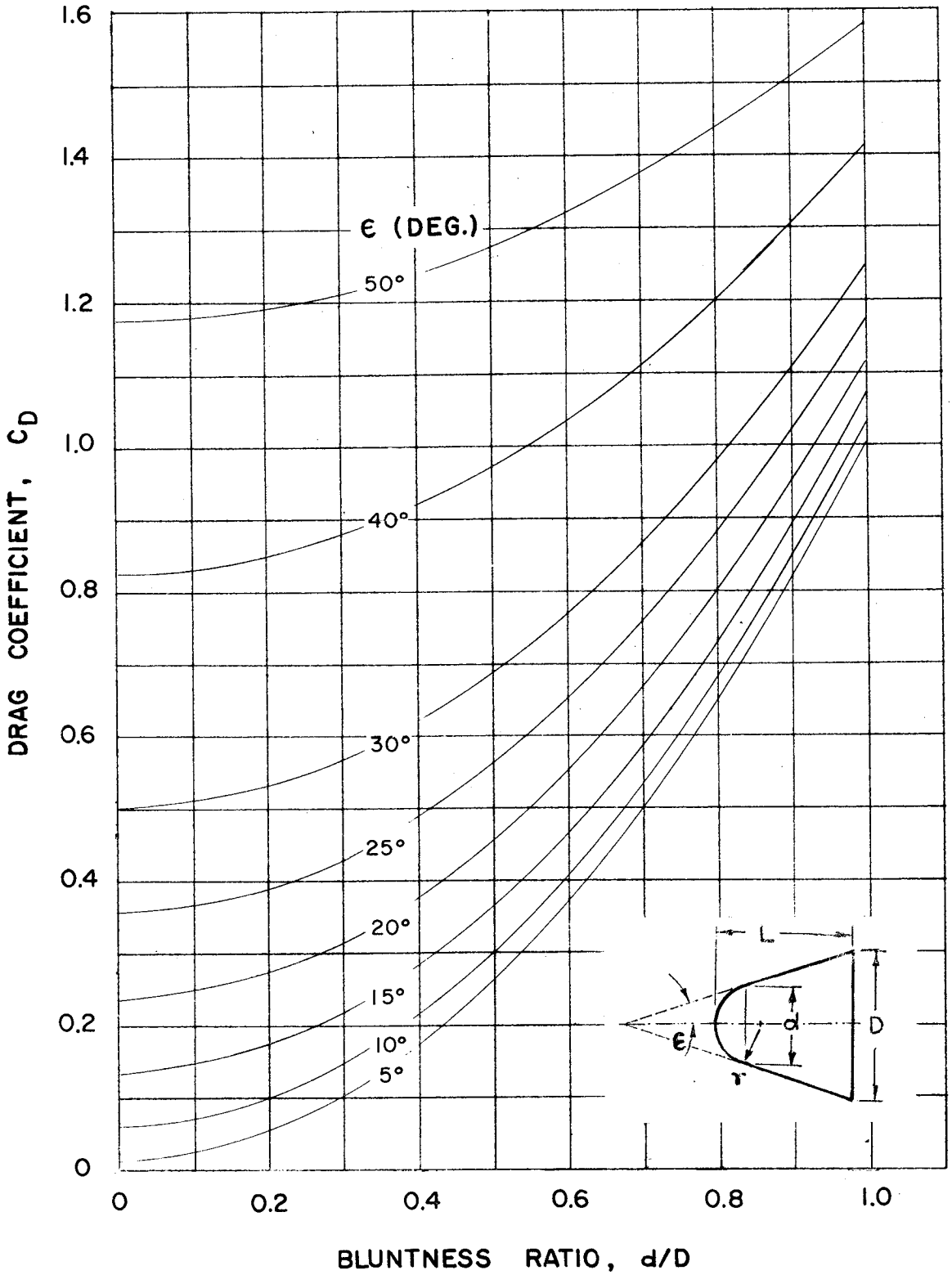

FIGURE A-5. HYPERSONIC NEWTONIAN WAVE DRAG FOR CONES OF VARYING GEOMETRY

REFERENCES

1. Felix, A. Richard; ABMA Report DA-TN-42-58; "Force Tests of a Related Family of Twenty Nose Cones for a Range of Mach Numbers from 0.47 to 1.93." July, 1958.

2. Marks, Alma S.; US AOMC-ARGMA-OML Report 648F; "Normal Force, Pitching Moment, and Center of Pressure of Several Spherically Blunted Cones at Mach Numbers of 1.50, 2.18, and 4.04." April, 1958.

3. Gendtner, W. J.; Convair Report ZA-7-017; "Sharp and Blunted Cone Force Coefficients and Centers of Pressure from Wind Tunnel Tests at Mach Numbers from 0.50 to 4.06." June, 1955.

4. NACA Report 1135; "Equations, Tables and Charts for Compressible Flow." Ames Research Staff; 1953.

5. Liepmann, H. W. and Roshko, A.; Elements of Gas Dynamics, John Wiley and Sons, Inc., New York; November, 1956.

6. Grimminger, G., Williams, E. P., and Young, G. W.; Journal of the Aeronautical Sciences, November, 1950; "Lift on Inclined Bodies of Revolution in Hypersonic Flow."